Experimental Photogrammetry of Lunar Images

GEOLOGICAL SURVEY PROFESSIONAL PAPER 1046–D

Prepared on behalf of the
National Aeronautics and Space Administration

Experimental Photogrammetry of Lunar Images

By SHERMAN S. C. WU *and* H. J. MOORE

APOLLO 15–17 ORBITAL INVESTIGATIONS

GEOLOGICAL SURVEY PROFESSIONAL PAPER 1046–D

Prepared on behalf of the National Aeronautics and Space Administration

An experimental photogrammetric study, using Apollo orbital photographs for geologic studies of the Moon and the exploration of the Moon and other planetary bodies

UNITED STATES GOVERNMENT PRINTING OFFICE, WASHINGTON : 1980

UNITED STATES DEPARTMENT OF THE INTERIOR

CECIL D. ANDRUS, *Secretary*

GEOLOGICAL SURVEY

H. William Menard, *Director*

Library of Congress Cataloging in Publication Data

Wu, Sherman S. C.
Experimental photogrammetry of lunar images.

(Apollo 15-17 orbital investigations) (Geological Survey professional paper ; 1046-D)
Bibliography: p. D22-D23.
1. Moon–Photographic measurements. 2. Moon–Maps. I. Moore, Henry J., joint author. II. United States. National Aeronautics and Space Administration. III. Title. IV. Series. V. Series: United States. Geological Survey. Professional paper ; 1046-D.
QB595.W8 559.9'1 80-607010

For sale by the Superintendent of Documents, U.S. Government Printing Office
Washington, D.C. 20402

Stock number 024-001-03300-3

CONTENTS

ILLUSTRATIONS

[Plates are in pocket]

TABLES

APOLLO 15–17 ORBITAL INVESTIGATIONS

EXPERIMENTAL PHOTOGRAMMETRY OF LUNAR IMAGES

By SHERMAN S. C. WU and H. J. MOORE

ABSTRACT

High-quality cameras capable of making reliable measurements and topographic maps were carried aboard the orbiting Command and Service Modules during Apollo missions 14, 15, 16, and 17. In addition to providing selenodetic control and topographic maps with scales of 1 : 10, 000, 1 : 50,000, and 1 : 250,000, photographs taken by these cameras can be used to obtain quantitative data for specialized scientific studies such as: (1) the relation between stereophotogrammetric measurements and illumination conditions, (2) measurement of structural deformation, (3) crater geometry and lunar landforms, (4) rheological properties of lunar flows, and (5) fine-scale lunar surface roughness.

Experimental photogrammetric studies have produced results applicable to the exploration of the Moon and other planetary bodies. Optimum illumination conditions for lunar stereophotogrammetric studies include sun elevation angles near 30°. Lower sun elevation angles result in excessive shadows, and much higher angles result in loss of scene contrast. For any given scene, local slope and albedo affect stereophotogrammetric measurements. Lunar results may be applied to other planetary bodies devoid of thick atmospheres.

Topographic maps prepared from vertical Apollo 15–17 mapping camera photographs can be prepared with contour intervals as small as 50 m depending on map scale, local roughness, illumination, and other conditions. Oblique photographs taken by the mapping camera can be used to prepare topographic maps with contour intervals of 50 m or larger. Panoramic camera photographs taken by Apollos 15–17 can be used to prepare topographic maps of fine-scale features with form-line intervals near 5 m under ideal conditions.

For scientific purposes, the small- and large-scale topographic maps can be used to determine subtle structural deformations of the lunar surface. Certain geologic features and shapes of small lunar landforms can be portrayed at a fine scale with an accuracy never before possible.

The geometry of lunar craters—the most ubiquitous lunar landform—has been determined using profiles and topographic maps prepared from Apollo 15–17 photographs with high accuracy. These profiles and maps required a revision of equations describing lunar craters.

Profiles of lunar volcanic and impact melt flows using the stereophotogrammetric method established the thicknesses and widths of the flows. When combined with theory and with lunar topographic maps to establish the gradient of the flow, it has been shown that the materials of mare flows had a yield strength about the same as basalt lava in Hawaii and that material of the flow of impact melt north of the crater King had a yield strength larger than the mare flow. Additionally, structural tilts of the maria after the mare flow formed were negligible, but some local warping occurred.

Stereophotogrammetric measurements on the high-resolution panoramic camera photographs of Apollos 15–17 and the lunar topographic camera photographs of Apollo 14 have been used to determine lunar surface roughness and slope-probability distributions at scale lengths of 17 to 25 m and larger. These data form a basis for comparison of the Apollo 14–16 bistatic-radar method of determining lunar surface roughness and slope-probability distributions at comparable scale lengths. The photogrammetric and radar methods agree on four major points: (1) lunar maria are smoother than uplands, (2) the magnitude of the algebraic standard deviations of slope-probability distributions for lunar maria are comparable for both methods, (3) maria appear rougher at small scale lengths than at large scale lengths, and (4) slope-probability distributions are typically semilogarithmic, but they vary and may be gaussian and complex.

Although the potential uses of Apollo photographs in special scientific studies have not been fully realized, existing studies employing the photographs and maps prepared from them have been profitable. Achievement of required mensuration for special scientific studies requires close coordination between the photogrammetrist and the user.

INTRODUCTION

In a substantial improvement over all previous Apollo lunar missions, the Command and Service Modules of the Apollo 15, 16, and 17 missions carried camera equipment capable of obtaining high-quality topographic and selenodetic data for the Moon from orbit. Equipment on each spacecraft included a mapping camera, a stellar camera, a laser altimeter, and a high-resolution panoramic camera. Accurate topographic measurements of the lunar surface in support of quantitative geologic studies can be made using the photographs returned to Earth by these later Apollo missions. Apollo 14 carried a lunar topographic camera (Hycon) in orbit from which quantitative topographic data could be obtained. Previous missions, as well as Apollos 14–17, carried Hasselblad cameras. Stereoscopic Hasselblad photographs of the lunar surface taken from orbit by the Apollo 11, 12, and 14 missions provided improved topographic data of selected features and were used in prelanding studies of the Apollo 16 landing site (Descartes).

This paper is one of four separately bound chapters summarizing Apollo 15–17 orbital investigations: (1) "Stratigraphy of Part of the Lunar Nearside" (Chapter

A, Wilhelms, 1980), (2) "Lunar Remote Sensing and Measurements" (Chapter B, Moore and others, 1980), (3) "Geometric Interpretation of Lunar Craters" (Chapter C, Pike, 1980), and (4) "Experimental Photogrammetry of Lunar Images" (Chapter D, this paper). This paper summarizes experimental photogrammetric studies done chiefly in support of special lunar research projects. Photogrammetric results described in this paper do not include the systematic topographic mapping being conducted by the Defense Mapping Agency (Kinsler, 1975) or the selenodetic system established by the U.S. Geological Survey and National Geodetic Survey (Doyle and others, 1976). Four categories of experimental photogrammetric studies are reported below: (1) the effect of illumination conditions on precision of measurements, (2) experimental topographic maps prepared to support specific topical studies and to demonstrate the capabilities of the photogrammetric method, (3) detailed profiling to be used in connection with specific topical studies, and (4) terrain analyses in support of the Apollo bistatic-radar experiment. These experimental photogrammetric studies demonstrate the value of the photogrammetric techniques in planetary exploration when suitable maps and photographs of the planetary surface are part of the exploration program.

Acknowledgments.—Results reported in this paper are based on work performed by the U.S. Geological Survey as part of NASA Experiment S–222 (Photogeology—Apollo 15–17; NASA contract T–1167B) on behalf of the National Aeronautics and Space Administration. The authors wish to express their appreciation to S. N. Hardee and J. Dixon of the Johnson Spacecraft Center, Houston, Tex. for their support and assistance in the experiment. Results reported in this paper were made possible because of the diligent and skillful efforts of Raymond Jordan, Francis J. Schafer, Bobby C. Philpott, and Gary M. Nakata of the U.S. Geological Survey. G. L. Tyler of Stanford University kindly furnished the results from the Apollo Bistatic-Radar Experiment.

CAMERAS AND PHOTOGRAPHY

Apollo cameras and photography used for photogrammetric purposes evolved from simple hand-held and bracket-mounted cameras in the Command Module and photographs taken through the spacecraft windows (Norman and others, 1969) to a sophisticated mapping camera system mounted in a scientific instrument module (Light, 1972). Photographs taken with Hasselblad cameras during the early Apollo missions were used to demonstrate the applicability of photogrammetry to mensuration and topographic mapping of the lunar surface (Norman and others, 1969; Wu, 1969, 1971). Apollo 14 was the first mission to obtain high-quality photographs suitable for photogrammetric purposes. The lunar topographic camera on board the Apollo 14 Command Module (Dietrich, 1971) was used to obtain data on fine-scale lunar roughness (Moore and others, 1975, 1976, 1980). Apollo missions 15, 16, and 17 carried the sophisticated mapping camera system in orbit (Dietrich and Clanton, 1972a, 1972b; McEwen and Clanton, 1973). In the mapping camera system, a 3-inch stellar camera was mounted at a 96° angle to the axis of a 3-inch mapping camera, and a laser altimeter capable of measuring slant range within± 2 m was alined with the mapping camera. This system has been used for establishing a selenodetic control network as well as topographic mapping (Doyle and others, 1976; Cannell and Ross, 1976; Kopal and Carder, 1974). A panoramic camera, carried on Apollo missions 15–17, obtained high-resolution stereophotographs that are useful for detailed studies. The cameras and photographs used to collect data in this report are discussed briefly below and listed in table 1.

LUNAR TOPOGRAPHIC CAMERA

The lunar topographic camera (45.5-cm focal length) (also called the Hycon camera) was carried aboard the orbiting Command Module of Apollo 14 to obtain high-resolution topographic data of the Apollo 16 landing site and the Apollo 14 landing site. A camera malfunction prevented acquisition of these data and resulted in the recovery of only 193 frames from altitudes of approximately 18 km extending from the east rim of the crater Theophilus to a point northwest of the crater Kant (El-Baz and Head, 1971). At a nominal spacecraft altitude of 20 km, each photograph, which has an 11.43 × 11.43-cm format, covers an area about 5.0 km on an edge. Photoscale is about 1:44,000. Stereoscopic coverage was achieved by overlapping consecutive frames by 60 percent, producing a base-height ratio of 0.095. Use of alternate pictures gives a base-height ratio near 0.19.

Photography taken with this camera had the highest resolution of all the Apollo missions flown previously, but higher resolutions were achieved by subsequent missions. Resolutions achieved by the lunar topographic camera are 62 optical pairs per millimeter at a tribar contrast of 2:1 with 3400 type film, which corresponds to a ground resolution of 0.7 m (H. W. Radin, memorandum for Bellcomm Inc., August 31, 1970).

The high resolution required image motion compensation, which was accomplished by rocking the camera in the direction of flight. Calibration of the camera using stellar methods yields a calibrated focal length of

TABLE 1.—*General features, films, and remarks for Apollo cameras used in experimental photogrammetric studies*

[After Dietrich (1971) and Dietrich and Clanton (1972a)]

Cameras	Features	Film size and type	Remarks
Lunar Topographic Camera	45.5-cm lens, vacuum platen, image-motion compensaton.	127 mm; type SO 349 high-definition aerial film, AEI 6; 3400 Panatomic-X black-and-white film, ASA 80.	Used to obtain high-resolution photographs of lunar surface near candidate Descartes crater landing site. Operating difficulties prevented scheduled convergent stereoscopic photography of the approach to the Descartes landing site, of the landed Lunar Module near Fra Mauro crater, and of the impact points of the Apollo 14 SIVB booster rocket stage and Lunar Module.
Mapping Camera	Electric; controls in CSM[1]; 7.62-cm-focal-length lens; 74° by 74° field of view; a square array of 121 reseau crosses, 8 fiducial marks, and the camera serial number recorded on each frame with auxiliary data of time, altitude, shutter speed, and forward-motion control setting.	457.2 m of 127-mm film type 3400 Panatomic-X, ASA 80.	The 11.43 by 11.43-cm frames with 78 percent forward overlap provide the first Apollo photographs of mapping quality. Data recorded on the film and telemetered to Earth will permit reconstruction of lunar-surface geometry with an accuracy not available with earlier systems.
Panoramic Camera	Electric; controls in CSM; 60.96-cm lens; 10°46′ by 108° field of view; fiducial marks printed along both edges; IRIG B time code printed along forward edge; data block includes frame number, time, mission data, V/h, and camera-pointing attitude.	1981.2 m of 127-mm film EK 3414.	11.43 by 114.8-cm images were taken looking alternately forward 12.5° then 12.5° aftward for stereopairs. Consecutive frames of similar tilt have 10 percent overlap; stereopairs, 100 percent overlap. Panoramic photographs provide high-resolution stereoscopic coverage of a strip approximately 330 km wide, centered on the ground track.

[1]Command and Service Module.

455.677±0.013 mm. A maximum radial distortion of 26 μm occurs at a radial distance of 72 mm and less than 10 μm within a distance of 40 mm for a standard format (Malhotra, 1970). Tangential distortions are 1.2 and 0.4 μm at distances of 72 and 40 mm, respectively.

MAPPING CAMERA

Mapping cameras (7.62-cm focal length) (also called metric or terrain cameras) were carried in the scientific instrument modules of the orbital spacecraft in Apollos 15, 16, and 17. Among the scientific objectives of the cameras were the development of a coordinate network of control points on the lunar surface with an accuracy of 10 to 15 m (Light, 1972) and the preparation of topographic maps (for example, Defense Mapping Agency, 1974a). Photographic coverage of the Moon by these cameras is extensive but constrained by the spacecraft orbits and illumination conditions of the Moon during the missions (Aeronautical Chart and Information Center, 1971; Defense Mapping Agency, 1972, 1973a). Importantly, some coverage was taken at oblique angles by rolling the spacecraft. At the nominal spacecraft altitude of 110 km, each photograph, which has an 11.43× 11.43-cm format, covers an area about 165 km on an edge. Photoscale is near 1:1.45 million. Stereoscopic coverage was obtained by overlapping consecutive frames 78 percent, producing base-height ratios near 0.33. Use of alternate frames increases the base-height ratio to 0.66.

Resolution of the cameras was 200 lines/mm at 1,000 to 1 contrast with film type 3400. Line-pair resolution of the ground is near 15 to 20 m at nominal altitude (National Space Science Data Center, 1972, 1973, 1974). Lens distortions are nominally less than 50 μm (Light, 1972). Film position and distortion can be controlled using images of 8 fiducial marks and a square array of 121 reseau marks engraved on the glass focal-plane plates used in each camera (Itek Corp., 1972). Calibration data for each camera are listed below.

Mission	*Camera serial No.*	*Calibrated focal length (mm)*	*Offset of principal point (mm)*
Apollo 15	003	76.080 ± 0.002	$x_p = -0.006, y_p = -0.002$
Apollo 16	005	75.936 ± 0.003	$x_p = -0.010, y_p = -0.004$
Apollo 17	203	75.842 ± 0.003	$x_p = -0.005, y_p = -0.007$

PANORAMIC CAMERA

The panoramic camera (60.96-cm focal length) is the highest resolution orbital camera employed by Apollo and combines high resolution with overlapping convergent photographs so that fine-scale measurements and detailed topographic maps may be made from photographs taken by the camera. In contrast with the

other Apollo cameras, the Itek optical bar panoramic camera is a fixed-focal-length direct-scanning camera producing cylindrical camera geometry. Scanning is accomplished mechanically with the scanning slit and center field of the lens operating as a unit. Use of the center field of the lens permits projection of the sharpest possible image onto the film. Photographic coverage of the Moon is extensive but constrained by the spacecraft orbits and illumination conditions of the Moon during the missions (Aeronautical Chart and Information Center, 1971; Defense Mapping Agency, 1972, 1973a). The frame format is 11.43 × 11.43 cm. Because of the cylindrical camera geometry, highest resolution is achieved along the ground track traced by the camera optical axis with minimum distance to the surface. At the nominal spacecraft altitude and 12.5° tilt in the direction of flight, the 11.43-cm film width corresponds to about 21 km along the ground track. Coverage in the crosstrack direction is about 330 km wide. Resolution decreases and coverage increases in the cross-track direction as tilts due to scanning increase symmetrically about the ground track. Photoscale along the track is near 1:185,000 for the nominal altitude. Stereoscopic coverage was obtained by alternately tilting the camera 12.5° forward along the track and 12.5° aftward along the track at 5-second intervals so that overlaps were 90 to 100 percent (National Space Science Data Center, 1972, 1973, 1974). Base-height ratios for nominal conditions were near 0.44, producing strong stereo-model geometry.

Resolution of the camera is 135 lines/mm at a contrast ratio of 2 : 1,180 lines/mm with medium-contrast targets, and 150 lines/mm with low-contrast targets (Itek Corp., 1967). Line-pair resolutions correspond to ground resolutions of 3.0, 2.0, and 2.5 m respectively at the center of scan. Because of the mechanical scanning, cylindrical geometry, and convergent stereopairs, distortions are complicated and more difficult to correct than those of frame cameras, and stereoscopic models are difficult. For these reasons, specially designed equipment such as the AS–11A stereoplotter (Ottico Meccanica Italiana, 1964) was required for mapping purposes. Some mensuration data such as profiling may be obtained with little or no error in directions parallel to the ground track using the AP/C plotter (Ottico Meccanica Italiana, 1966). The panoramic cameras used during each of the Apollo missions were completely calibrated (Itek Corp., 1967), and calibrated focal lengths are listed below.

Mission	*Lens serial No.*	*Camera No.*	*Calibrated focal length (mm)*
Apollo 15	N–54	003	609.752 ± 0.025
Apollo 16	N–45	005	609.524 ± 0.025
Apollo 17	N–53	?	609.676 ± 0.025

Some of the panoramic camera photographs of the Apollo 17 mission near the area of the lunar crater Euler were obtained without rocking the camera to produce the 25.0° convergence angle. For this photography a 10 percent overlap of consecutive frames was obtained, giving base-to-height ratios less than or close to 0.1. Here stereomodel geometry is weak, and mensuration is substantially poorer than for the nominal panoramic photographs.

METHODS AND PROCEDURES

EQUIPMENT AND MATERIALS

Photogrammetric equipment used in the mensuration and topographic mapping in this report were the AP/C (Ottico Meccanica Italiana, 1966) and the AS–11A (Ottico Meccanica Italiana, 1964) analytical stereoplotters. Both plotters are controlled by computers. The plotters are very flexible in accommodating a wide range of photographic geometries, principal distances, and base-height ratios, and lens distortion and lunar curvature can be corrected by the computers. Topographic maps prepared from panoramic camera photographs require the AS–11A plotter, but the AP/C can be used with panoramic camera photographs for profiles parallel to and measurements near to the groundtrack. Cross-track profiles from panoramic camera photographs prepared using the AP/C are curved because of the cylindrical geometry described above. Both plotters have a least significant reading capability of 1 μm, and repeated measurements have a precision near ± 2 μm. When combined with the scale and base-height ratios of the mapping camera photographs, this precision translates to ±7.5–10 m for a variety of mapping camera photographs (Wu, 1976). Nominal values for each camera are listed in table 2.

In the studies, second-generation master positive transparencies prepared from the original negative were used in the plotters. These transparent positives are the best quality reproductions available in original format size and provide photographs with minimal loss of the original resolution. Probable errors in elevation measurements are interpreted in terms of nominal photograph resolution (Gardner, 1932) in table 2.

CONTROL AND LEVELING

Because the selenodetic control points were not available at the time of part of the photogrammetric processing, stereomodels of mapping camera photographs were oriented and leveled using photosupport data and existing small-scale topographic maps. For setting up models of panoramic camera photographs, control information was obtained from stereomodels of

TABLE 2—*Nominal errors in elevation related to Apollo photographs and analytical stereoplotters*

Cameras	Scale ($\times 10^{-6}$)	Resolution (lines/mm)	Base-height ratio	Plotter precision (μm)	Plotter precision in elevation (m)	Photograph probable error (μm)	Probable error in elevation (m)
Lunar topographic	0.044	62	0.19	±2	0.15	3.2–4.0	0.71–0.88
Panoramic	.185	180	.44	±2	.64	1.1–1.3	.47– .56
Mapping	1.45	200	.33	±2	8.6	1.0–1.2	4.3 –5.4

mapping photographs covering the same area. In the case of the lunar topographic camera photographs, model orientation information was sometimes obtained from Lunar Orbiter pictures and data (National Space Science Data Center, 1969). In some cases, where the geology of a local area was of interest and where no information was available, such techniques as assuming a mare surface to be level or the rim of a large crater to be level were used.

METHODS OF MEASUREMENTS

For map compilation or profile plotting, after a stereomodel is obtained, regular photogrammetric procedures are followed to plot measurements. However, for the support of terrain analysis, specifically for the study of slope-probability distributions of the lunar surface, which will be described in detail in this report, statistical profiles are measured in a model along linear traverses using a constant horizontal distance between consecutive points. Each profile contains at least 500 points. At each point three to five readings were taken. A sample area was chosen that is representative of a surface geologic unit. The slope-probability statistics then provide a quantifier for that type surface or that geologic unit.

PRECISION OF MEASUREMENT

The level of detail that can be achieved in preparing profiles and topographic maps from Apollo stereophotographs depends on the standard error in elevation measurements (σ_h),[1] which is the product of photograph scale or its reciprocal-scale factor (S_p), the height-base ratio (H/B), and the standard error of parallax measurement (σ_x) (Doyle, 1963; Light, 1972). Scale factors and height-base ratios using Apollo photographs with suitable plotters are generally ideal to very good. The standard error of parallax measurement is related to a number of factors such as lens distortions, photograph quality, scene contrast, and the person who measures parallax. Scene contrast is related to surface roughness or patterns and illumination conditions. The wide variety of illumination conditions of Apollo photography combined with the reflective properties of the lunar surface offered an opportunity to discover the relation between illumination and the standard error in measurement. Extensive studies using mapping camera photographs have been made relating standard error in measurements with variable illumination conditions and, to some extent, with slopes (Wu, 1976). Data on standard errors in measurement for the lunar topographic camera and panoramic camera photographs are limited, but some results are reported here (see also Wu and others, 1973).

[1]When experimentally determined, the standard error in elevation measurement is designated S_E.

MAPPING CAMERA PHOTOGRAPHY

Standard errors in measurement for Apollo mapping camera photographs correlate strongly with the illumination conditions (Wu, 1976). When sun elevation angles are less than about 10°, large areas of the rugged parts of the Moon are covered by shadow. This condition precludes measurements in deep shadows, and standard errors in diffuse shadows tend to be large. Photographs taken with sun elevation angles larger than 30° show increasing average standard errors in measurements because scene contrast is reduced by the large relative increase in reflected sunlight or heiligenschein at large incidence angles (Wildey, 1972).

Regression fits were made to the data in the form

$$Y = \alpha + \beta X + \gamma X^2,$$

Where Y is the standard error in measurement, X is sun elevation angle, and α, β, and γ are coefficients listed in table 3 for each mission and the combined missions. The regressions, exclusive of Apollo 16, show

TABLE 3.—*Coefficients of regression curves determined from all standard errors and local sun elevation angles for each measured point*

Coefficients of regression curve	Apollo 15	Apollo 16	Apollo 17	Combined Apollo 15–17
α	7.70	6.91	10.84	8.48
β	.0361	.0938	−.206	−.561
γ	.00149	.000194	.00348	.00181

a tendency for the minimum standard error in elevation measurement to occur near a sun elevation angle of 30° (fig. 1). Similar results are obtained where local slope is taken into account (fig. 1). Results in detail are described in an investigation on illumination and measurement precision for lunar photography (Wu, 1976).

Although these studies clearly show that sun elevation angles near 30° are optimal for stereophotogrammetry, the effects of the photometric function, surface albedo, and height-base ratio have not been carefully studied.

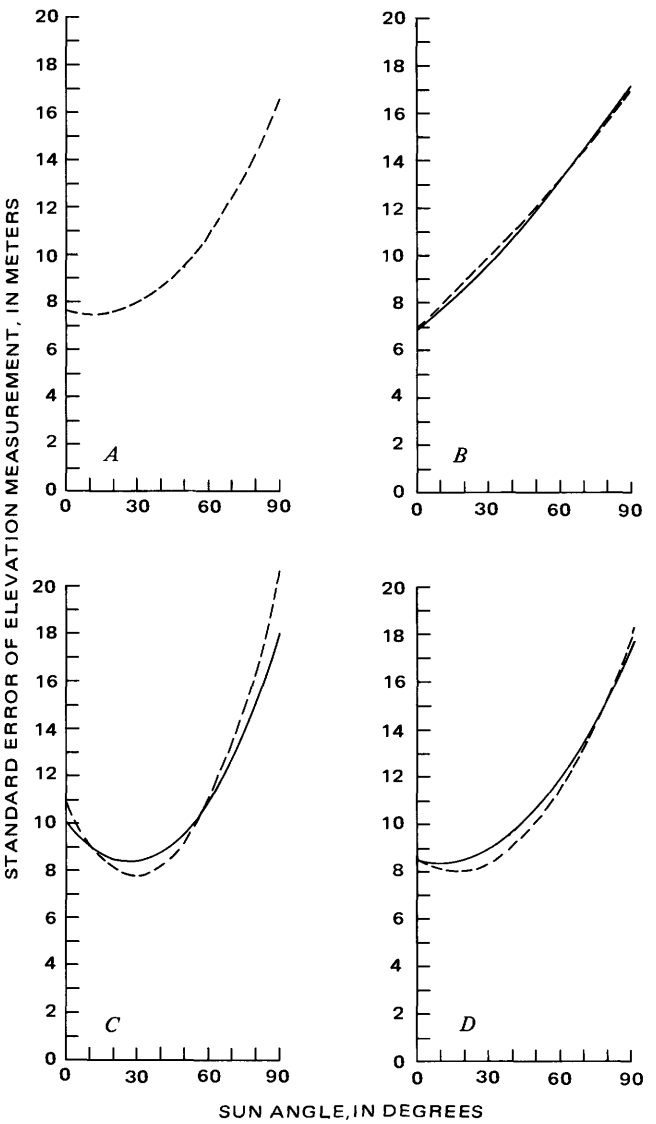

FIGURE 1.—Regression curves determined from standard error in elevation measurement (S_E) and local sun elevation angles (dashed lines); standard error in elevation measurement and local sun elevation angles corrected for surface tilt (solid lines): (*A*) Apollo 15, (*B*) Apollo 16, (*C*) Apollo 17, and (*D*) combined data.

PANORAMIC AND LUNAR TOPOGRAPHIC CAMERA PHOTOGRAPHY

As part of the measurements for surface roughness and slope-probability distributions at the fine scale, average standard errors in measurement were computed for 500 to 1,000 points on lunar topographic and panoramic camera photographs. Standard errors in elevation measurements (S_E) for each point were estimated from the readings. Averages of the standard error in measurement, tabulated below, represent an estimate for those photographs.

Camera	*Average of standard error of average of measurements*	*Number of standard errors in average*
Lunar topographic	0.7 ± 0.4 m	9
Panoramic	.9 ± .2 m	15

TOPOGRAPHIC MAPS

Apollo mapping and panoramic camera photographs provide accurate data on the morphology of lunar craters and other features with subtle relief. Topographic mapping of the Moon at 1 : 250,000 scale with mapping camera photographs has been extensive (Kinsler, 1975). Contour intervals of 100 m are standard for these maps, and in some cases supplementary contours with a 50-m interval are given (see for example Defense Mapping Agency, 1975). Scales and contour intervals of maps prepared from panoramic camera photographs vary depending on the features portrayed. The largest scale maps are 1 : 10,000 with a 10-m contour interval and 5-m supplementary contours (see for example Defense Mapping Agency, 1974d). These contour intervals are entirely consistent with the capabilities of the cameras and the quality of the photographs. Acceptable contour intervals are three or more times the standard error in elevation (3 σ_h) and fall within or close to the combined errors of resolution, instrument errors, and errors measured experimentally.

Some experimental topographic maps were prepared by the U.S. Geological Survey to test the capability of the photography and to obtain scientific data on a timely basis and with sufficient detail. Purposes of the maps included support of the bistatic-radar studies, dimensions of craters, and miscellaneous geologic studies. Table 4 summarizes the maps prepared and their use. Although not considered in detail here, two maps prepared from Apollo 12 Hasselblad photographs are included in the table.

VERTICAL MAPPING CAMERA PHOTOGRAPHY

A topographic contour map of the scablands region north of the Aristarchus Plateau was compiled from

vertical mapping camera photographs (fig. 2). The photographs were taken under a number of favorable conditions such as (1) vertical optic axes, (2) a large base-height ratio (0.4), and (3) good sun illumination conditions (sun elevation angle of 12°). In addition, horizontal and vertical control was available from the

TABLE 4.—*Experimental topographic maps prepared in support of Photogeology-Apollo 15–17 (NASA Experiment S–222)*

Map name or title	Location		Scale	Contour interval (m)	Photographs used	Plotter used	Map compiler	Use
	Long.	Lat.						
Herschel	2° W.	6°S.	1:200,000	200	AS12–8069,–8070 80-mm Hasselblad	AP/C	R. Jordan	Support Bistatic-Radar Experiment, study of large-scale lunar roughness.
Lansberg	27° W.	2° S.	1:200,000	200	AS12–8093,–8094 80-mm Hasselblad	AP/C	do	Do.
Scablands north of Aristarchus plateau	53° W.	28° N.	1:100,000	50	AS15–Map–2483,–2484	AP/C	do	Geologic study of Aristarchus region.
Do	53° W.	28° N.	1:50,000	10	AS15–Pan–2342, –2347; AS15–Pan–2344, –2349	AS–11A	do	Do.
Alphonsus	2° W.	12° S.	1:250,000	200	AS16–Map–2477,–2478	AP/C	G. Nakata R. Jordan	Demonstration of use of oblique mapping camera photographs in preparation of topographic maps.
Southeast Krieger area	45° W.	28° S.	1:10,000	10	AS15–Pan–0320,–0325	AS–11A	R. Jordan	Study of morphology of secondary-impact craters from Aristarchus.
Mare dome northeast of Aristarchus plateau	49° W.	31° N.	1:15,000	10	AS15–Pan–0332,–0337	AS–11A	do	Study of morphology of lunar domes.
North of Diophantus	34° W.	28° N.	1:50,000	20	AS15–Pan–0290,–0295	AS–11A	do	Study of crater morphology. Provides data on dimensions of smallest craters photographed by Apollo from orbit.
Domed crater in crater Aitkin	168° W.	15° S.	1:15,000	10	AS15–Pan–1915,–1920	AS–11A	do	Study of morphology of lunar domes.
Lee-Lincoln Scarp (strip map)	30° W.	20° N.	1:25,000	10	AS17–Pan–2752,–2757	AS–11A	do	Study of structural deformation of lunar surface.

FIGURE 2.—Vertical Apollo 15 mapping camera photograph 2483 of scabland region north of Aristarchus plateau. Photograph is one of a stereoscopic pair used to make topographic map in plate 1.

1 : 250,000-scale maps "Nielsen" and "Freud" (Defense Mapping Agency, 1974e, f). For these reasons it was a good model to use to determine the smallest contour interval that could be obtained with this type of photograph. As shown in plate 1, a 50-m contour interval can be obtained from the Apollo mapping camera photographs. This map, combined with one prepared from panoramic camera photographs, was used to detect warping of the lunar surface that occurred after the formation of the rilles. Figure 2 is one of the mapping camera photographs used in compiling the topographic map in plate 1.

OBLIQUE MAPPING CAMERA PHOTOGRAPHY

An experiment has demonstrated that valuable topographic data can be obtained from high oblique photographs (Wu and others, 1972). As shown in figure 3, the crater Alphonsus was covered by Apollo 16 mapping camera photographs 2477 and 2478. The high tilt (40°) of these photographs was enough to include the horizon. A topographic form-line map was compiled from this model in the AP/C plotter (fig. 4). In spite of the large tilt angles, this model has a 0.35 base-height ratio. The average standard error of repeatability of elevation measurements within the mapped area was near 11 m. Thus it is possible to attain a contour interval of 50 m. Because the photographic support data for the Apollo 16 photographs were not available at the time this test was made, the model was scaled using Lunar Orbiter support data (LO IV H–108) and leveled assuming that the floor of Alphonsus was level.

PANORAMIC CAMERA PHOTOGRAPHY

Very detailed topographic information of subtle landforms and small craters can be obtained from the panoramic camera photographs. Several experimental topographic maps were compiled of geologically significant features on the lunar surface. Some of these topographic maps are described in the following sections. All of the model geometries from which these maps were compiled are similar in that they all have a 25° convergent angle, which gives a strong base-height ratio of 0.44, and they all have from 90 to 100 percent overlap. The model scales range from 1 : 150,000 to

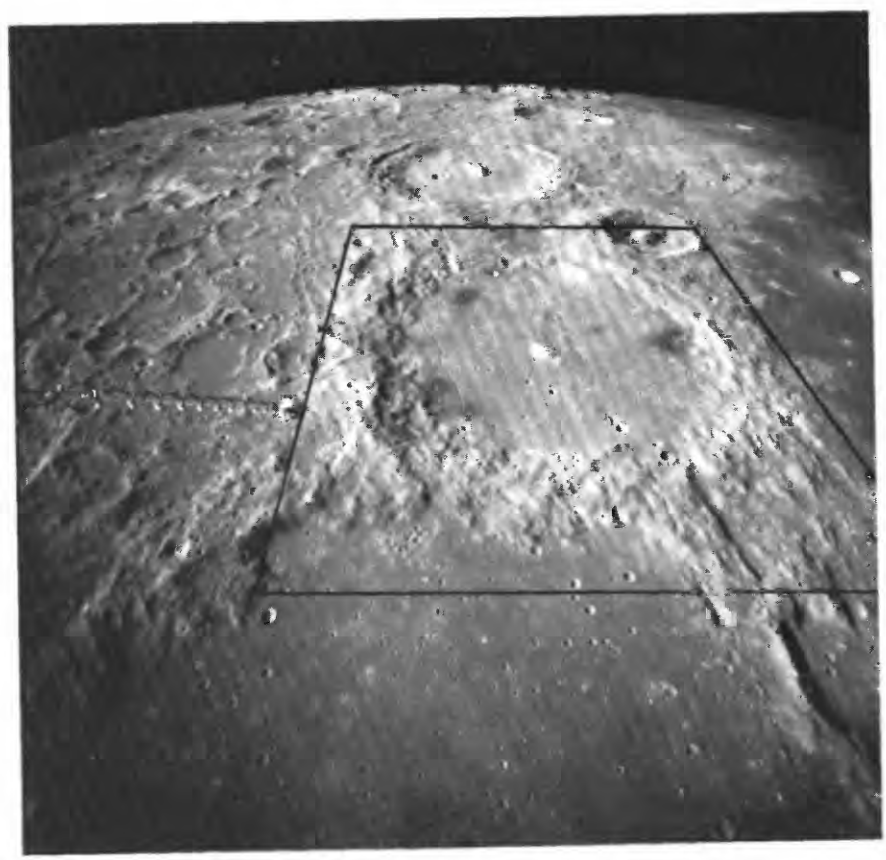

FIGURE 3.—Apollo 16 mapping camera photograph 2477 is one of the photographs used in compiling the topographic map shown in figure 4. Outline shows location of boundaries of map in figure 4.

1 : 200,000, from which a 1 : 10,000 map scale is quite easily obtainable on an analytical plotter.

One experimental topographic map of an area southeast of Krieger was compiled from Apollo 15 panoramic photographs (pl. 2). This map demonstrates that a scale as large as 1 : 10,000 with a 5-m form-line interval can be obtained from a model of panoramic photography. To obtain control information to orient this model, a

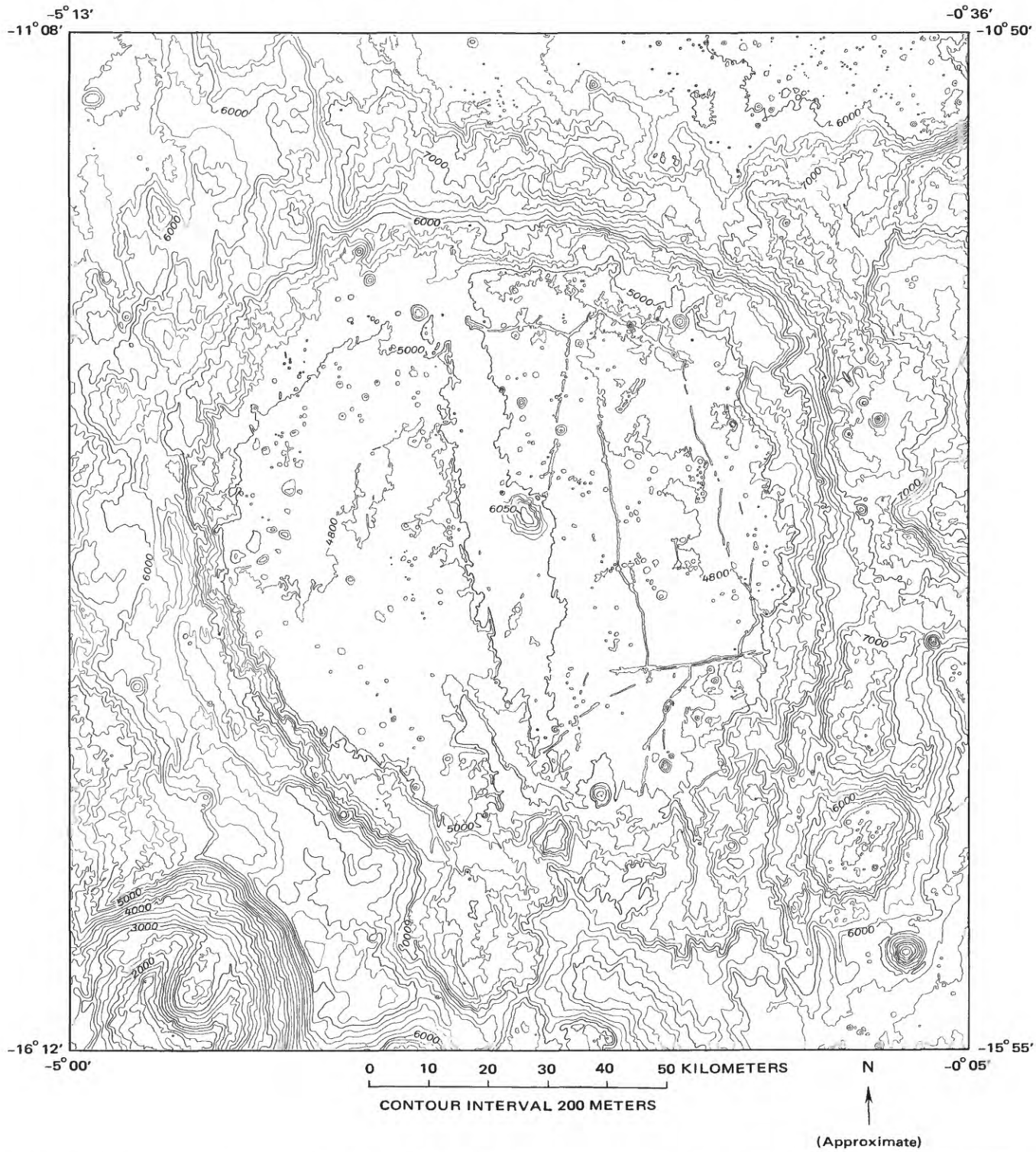

FIGURE 4.—Contour map of Alphonsus compiled from oblique Apollo 16 mapping camera photographs 2477 (see fig. 3) and 2478. Map prepared under NASA contract T5874A.

model from Apollo 15 mapping camera photographs (numbers 2478 and 2479) was set up on the AP/C analytical plotter. The scaling information for this mapping camera model was obtained from the photographic support data, and the leveling was accomplished by selecting elevations from Lunar Topographic Orthophotomap LTO 39Al, Kreiger (Defense Mapping Agency, 1973b). Secondary craters portrayed on this map were produced by Aristarchus some 150 km south and form part of the data set on lunar crater geometry (Pike, 1974, 1980). Secondary crater diameters, depths, rim heights, circularity, and ejecta symmetry can be measured on the map.

Another topographic map (pl. 3) illustrates that subtle features such as lunar domes can be accurately portrayed using panoramic camera photographs. The dome has a mere 60 m of relief and is seen with vivid clarity on low-sun photographs. On the 1 : 250,000-scale Lunar Topographic Orthophotomap (LTO) Krieger (Defense Mapping Agency, 1973b), only one contour is present around the dome because of the 50-m contour interval. Thus, subtle features barely detectable in topographic maps prepared from mapping camera photographs can only be portrayed in detail by stereophotogrammetry from panoramic camera photographs.

A topographic map of the Delisle-Diophantus area compiled on the AS–11A plotter is included on the area covered by LTO Delisle (Defense Mapping Agency, 1974a) (pl. 4). Dimensions of small craters derived from this map represent the best data in the sample on very small lunar craters used in establishing the geometry of lunar craters (Pike, 1974). The nature and amount of filling of Rima Brahms (the sinuous rille that transects the map) by ejecta from two larger craters to the north and south (Delisle and Diophantus) can be measured. Some data on the morphology of ejecta blankets can be obtained from this map.

PROFILES

Some topical studies of the Moon require carefully and specially prepared profiles in order to achieve the objectives of the study, and close coordination between the user and photogrammetrist is required. Pioneering efforts were conducted with Apollo 10 Hasselblad photographs to compare profiles derived with photogrammetric and photoclinometric techniques (Lucchitta, 1971), to study mass wasting (Pike, 1971b), and to demonstrate the photogrammetric method for lunar research (Wu, 1969, 1971). Subsequently, photographs taken with the photogrammetric quality cameras of Apollo 15, 16, and 17 were used to make profiles for specific studies. Two such examples are the quantitative studies of crater dimensions and lunar flows.

CRATER GEOMETRY

Profiles of craters were very important in the early phases of studies employing Apollo mapping camera photographs when carefully controlled maps prepared with them were not yet available. Profile data along with geologic interpretation resolved the controversy of the origin of the previously enigmatic crater Linné (fig. 5), which turned out to be an ordinary albeit very fresh impact crater (Pike, 1973b, 1980). Topographic analyses of 25 farside craters (table 5) 1.6 to 275 km across showed that the craters do not differ in shape from nearside craters and their shapes were more consistent with an impact origin than a volcanic origin (Pike, 1973a, 1980). It was also shown that shapes of farside craters measured with stereophotogrammetry were more consistent with lunar nearside craters than those measured using photometry. Because carefully controlled maps were not available for these early studies, orientations of stereomodels were accomplished with sufficient accuracy in a variety of ways: (1) For craters superposed on maria, surrounding surfaces were assumed to be level, (2) for large craters, their flat floors were taken as level, and (3) for some craters, Lunar Orbiter data were used (National Space Science Data Center, 1969). Stereophotogrammetric profiles prepared by the U.S. Geological Survey and measurements obtained from Lunar Topographic Orthophotomaps (for example Defense Mapping Agency, 1974a) prepared from Apollo mapping and panoramic camera photographs have resulted in a revision of depth-diameter relations of lunar craters (Pike, 1974) and have revealed discrepancies of some pre-Apollo data (Pike, 1972).

LUNAR FLOWS

Detailed profiles of a flow lobe (figs. 6 and 7) in Mare Imbrium were a necessary part of a study of the rheological properties of the flow and tectonic deformation in the general area (Moore and Schaber, 1975). In this study it was shown that the yield strength of the lunar flow was comparable to measured values of molten lava in Hawaii and that little or no post-flow regional tectonic tilt had occurred, although there was evidence for local warping. Both carefully controlled maps and high-resolution Apollo panoramic camera stereophotographs were required for the study. Relief of the flows is 7–20 m, comparable to the standard error of elevation measurement of the mapping camera photographs. In contrast, panoramic camera photographs have a standard error of measurement near 1.0 m (Wu and others, 1973). Profiles were measured using the AP/C stereoplotter because the desired profiles were very nearly parallel to the ground track. Cross-

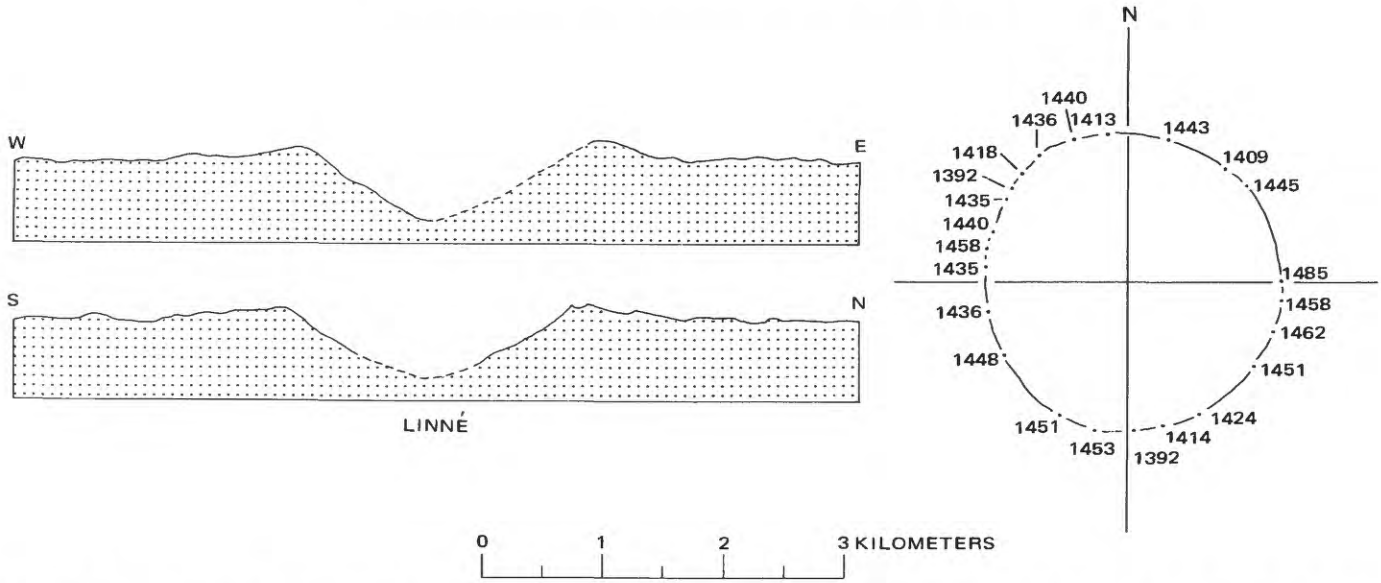

FIGURE 5.—Profiles and rim-crest elevations of Linné; dashed lines indicate areas in shadow; horizontal and vertical scales are equal. Numbers to right indicate altitudes in meters above an arbitrary datum. Linné was a famous "problem" crater which Apollo 15 photographs revealed to be an extremely fresh impact crater (Pike, 1973b, 1980). Profiles and rim-crest elevations prepared by R. Jordan, U.S. Geological Survey, Flagstaff, Ariz. from Apollo 15 mapping camera frames 0408 and 0407.

TABLE 5.—*Profiles prepared for studies of crater dimensions*

[From Pike, 1972, 1973a, 1980]

Name or location	Rim diameter (km)	Depth (m)	Outer rim height (m)	Mapping camera frames AS-15 metric	Number of profiles
Farside craters–Apollo 15					
In Sklodowska	1.6	300	95	1875 & 1874, 1968 & 1967, 1970 & 1969, 1966 & 1965	2
Do	2.8	550	125	do	--
Do	128.0	4,500	1,850	do	--
In Hirayama	3.5	500	175	0919 & 0917	4
In Tsiolkovsky	4.9	950	100	0480 & 0479	1
Do	190.0	4,700	1,750	0482 & 0481, 1569 & 1568, 1571 & 1569, 1573 & 1571, 1575 & 1573, 1576 & 1575, 1714 & 1713	2
In Hilbert	6.0	950	150	1589 & 1588, 1727 & 1726, 1729 & 1728, 1732 & 1731, 1867 & 1866	2
Do	17.0	1,800	400	do.	
Do	178.0	4,100	1,500	do.	
In Pasteur	9.9	1,100	105	0910 & 0908	4
In Saha	15.7	880	280	0333 & 0332	2
In Gagarin	16.0	1,350	650	0293 & 0291, 0295 & 0293, 0098 & 0097, 0289 & 0288, 0291 & 0289, 0297 & 0295, 0299 & 0297, 0300 & 0297, 0102 & 0101	4
In Gagarin	17.0	1,700	450	do	4
On western rim of Gagarin	26.0	2,600	725	do	5
In Gagarin	275.0	5,375	(3,350?)	do	
Farside craters–Apollo 15—Continued					
Izsak	33.2	3,400	1,025	1859 & 1858	2
Gilbert M	34.0	3,100	850	1072 & 1071	2
Gansky	44.0	3,550	950	1057 & 1055	2
South of Saha	50.5	3,640	1,380	0333 & 0332	2
Schorr	53.5	3,700	730	2230 & 2229	2
Ritz	59.0	3,750	1,800	1879 & 1878	2
In King	71.0	3,830	1,690	1557 & 1558	2
In Langema-K	110.0	4,370	880	0123 & 0122, 0122 & 0121	2
In Curie	158.0	3,850	1,500	2368 & 2369, 2366 & 2367, 2365 & 2364	2
Mare craters–Apollo 15					
Linné	2.5	600	130	0407 & 0408	2
Timocharis	38	3,000	850	1830 & 1831	2
Langrenus	135	4,500	1,500	2108 & 2109, 2390 & 2391, 2390 & 2389, 0121 & 0122, 0123, 2261 & 2662	4
Mare craters–Apollo 16					
Mädler	27.0	2,830	885		
Langrenus B	32.0	1,865	470		
Isidorus	36.8	2,110	830	2971, 2972	1
Capella	38.8	2,800	895		
King	71.0	3,830	1,690	Pan 5000 & 5005	8
Mare craters–Apollo 17					
Pierce B	11	2,040	460	0287–0291	3
Pierce	20	2,160	640	do	
Proclus	28	4,040	1,790	0293–0296	3

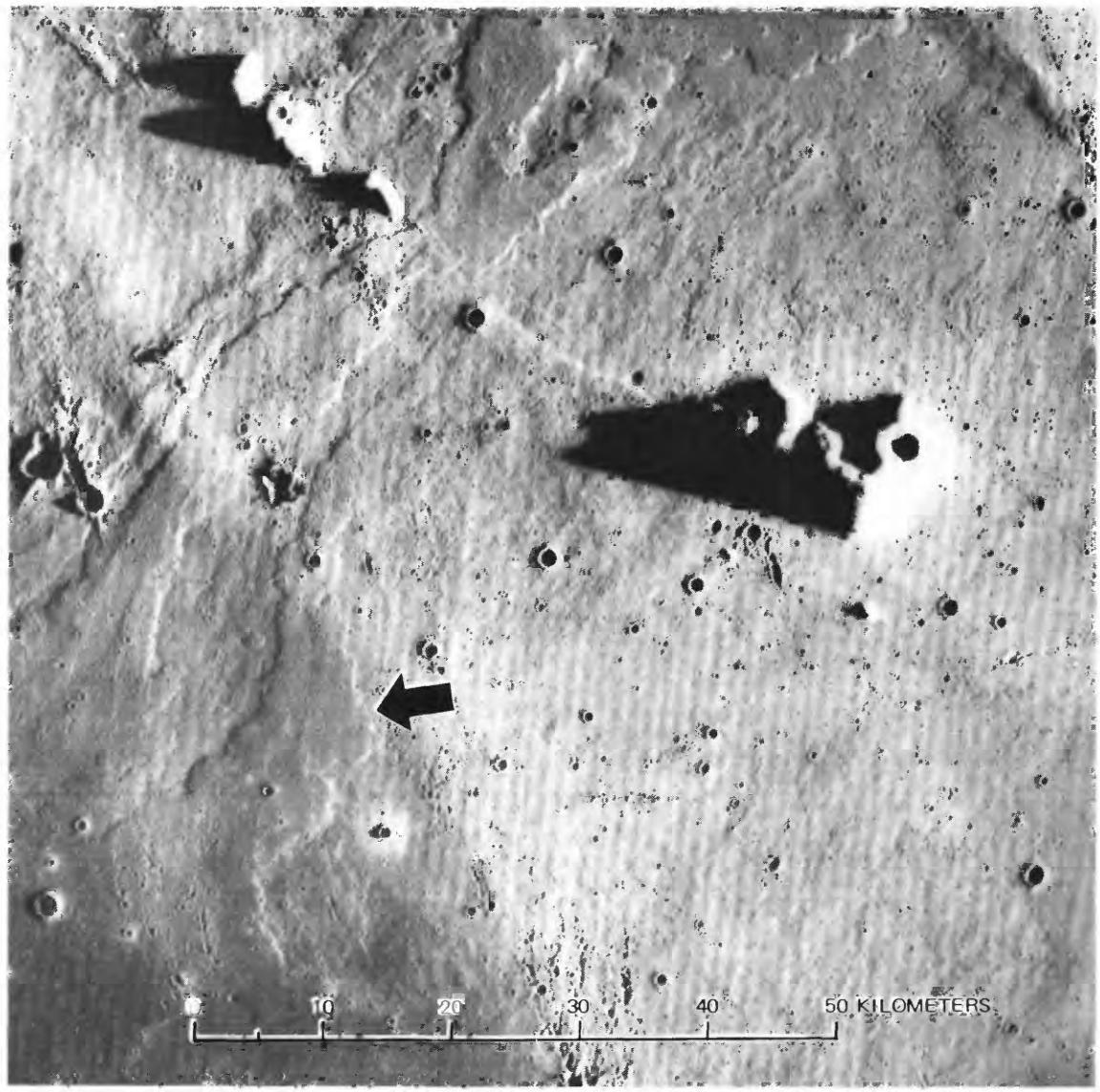

FIGURE 6.—Lava flows in Mare Imbrium. Flow lobe in figure 7 indicated by arrow at lower left. Relief of flows is generally small (7–20 m), requiring careful techniques and Apollo panoramic camera photographs to obtain detailed profiles. Rectified oblique photograph; sun is to right. (Apollo mapping camera frame 1556.)

track profiles showed the curvature expected from camera geometry and were not used. Approximate leveling was achieved using an existing base map (Defense Mapping Agency, 1974b). The profiles appear to be tilted a large amount (fig. 7) because of the large vertical exaggeration, but tilts are in reality very small, less than 0.4° in every case. In an independently measured profile (not shown in fig. 7) along C–C', the tilt was in the opposite direction. Thickness estimates remained the same. Because of the artificial tilts and obvious curvature in the cross-track profiles, gradients in the direction of flow for the rheological and tectonic study were obtained from a map at a scale of 1 : 250,000 prepared from mapping camera photographs (Defense Mapping Agency, 1974b). The 100-m contour interval of the map was much too large for estimating the thickness of the flow.

Profiles of a flow lobe in the basin just north of the crater King (fig. 8) were also analyzed in conjunction with a quality 1 : 250,000-scale map (Defense Mapping Agency, 1974c) to study the rheology of flows in the lunar highlands (Moore and Schaber, 1975). Yield strengths for this highland flow were much larger than those of the Imbrium volcanic flow and consistent with a higher silica content of the highland flow. Additionally, topographic data showed that frictional sliding could not account for the movement of the flow mass.

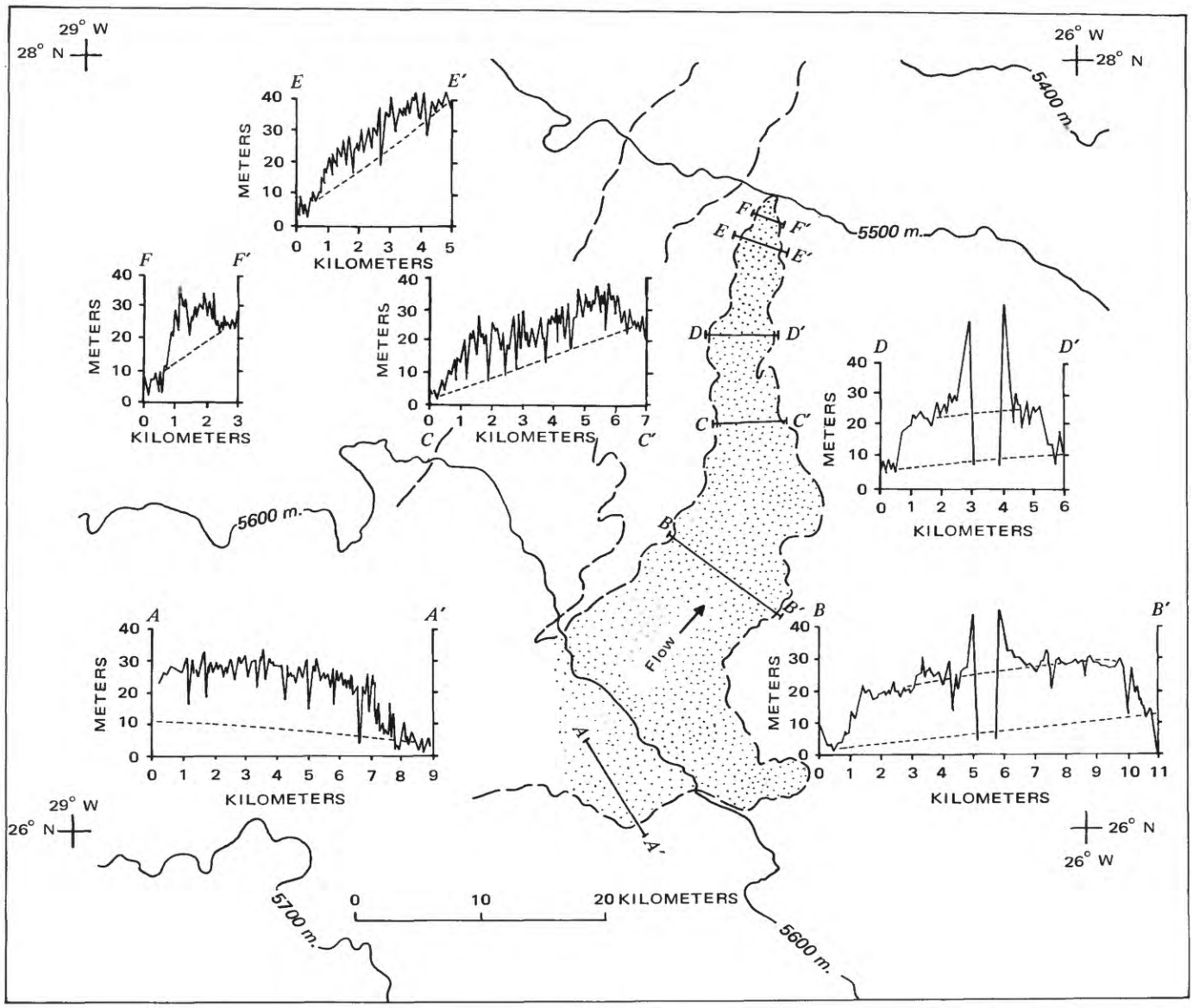

FIGURE 7.—Map and profiles of Imbrium flow lobe. Solid lines on map are contours of elevation taken from Lunar Topographic Orthophotomap, La Hire; LTO 40A 4 (250) (Defense Mapping Agency, 1974a); dashed lines delineate flow base; stipples indicate flow that was the subject of a topical study (Moore and Schaber, 1975). Solid lines of profiles delineate present surface; short dashes indicate apparent base of flow and approximate top of flow in some profiles; craters disrupt centers on profiles D–D' and B–B'; vertical exaggeration of profile is 100×. Profiles prepared by R. Jordan and B. C. Philpott, U.S. Geological Survey, Flagstaff, Ariz., from Apollo 15 panoramic camera frames 0270, 0275, 0272, and 0277.

LUNAR SURFACE ROUGHNESS

The Apollo orbital missions provided two independent methods of estimating surface roughness: radar and photogrammetry. Command and Service Modules of Apollo 14, 15, and 16 conducted bistatic-radar experiments which resulted in estimates of surface roughness from areas 10 to 20 km across along the gound tracks (Howard and Tyler, 1971). Slope-probability distributions are also obtained at two wavelengths by summing the echoes over 2° intervals (Parker and Tyler, 1973). Roughness and slope-probability distributions measured on positive transparencies of stereoscopic photographs taken by the lunar topographic, mapping, and panoramic cameras provide a basis for comparison of the radar and photogrammetric methods. Earlier studies compared the results of the Explorer 35 bistatic-radar experiment with 220-cm wavelength radio transmissions (Tyler and Simpson, 1970) and photoclinometric studies on Earth-based photographs (Tyler and others, 1971). Preliminary studies of lunar surface roughness using stereophotogrammetry began during Apollo 10 and employed Has-

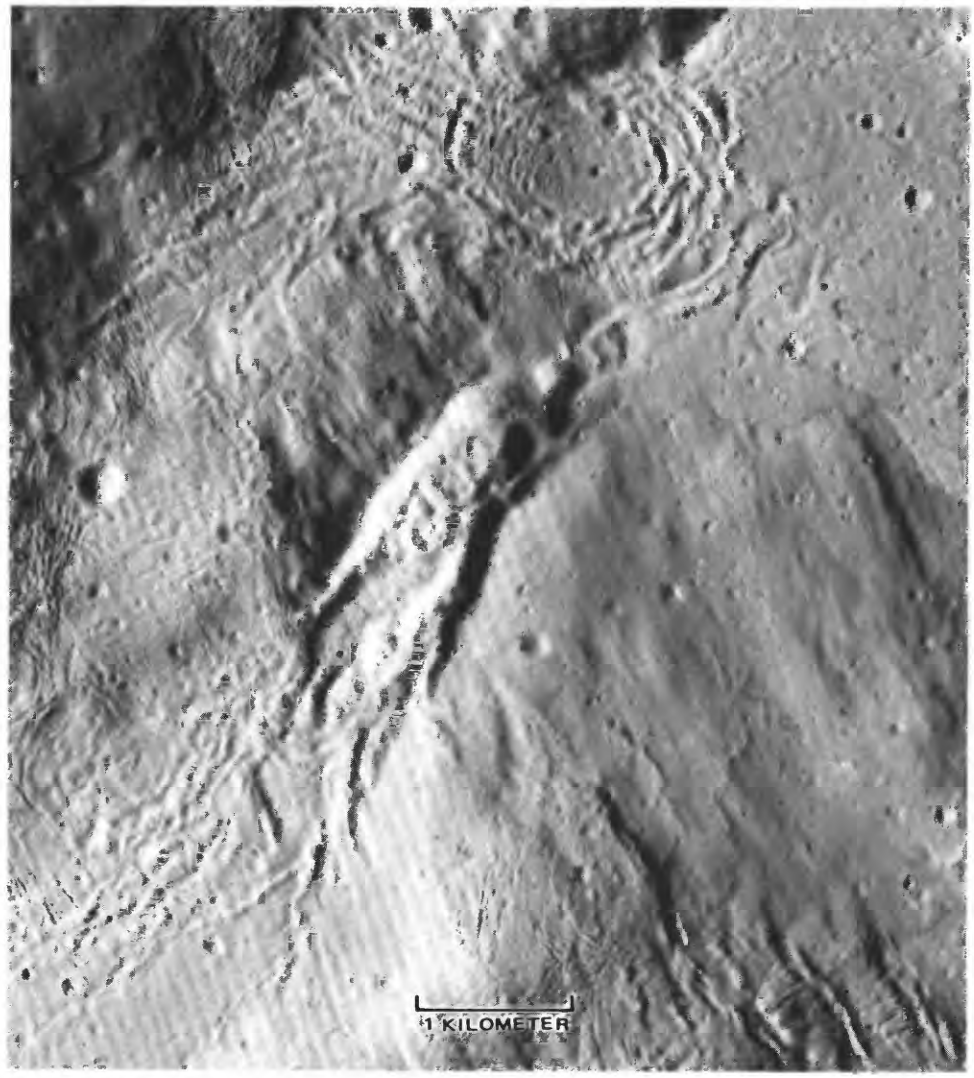

FIGURE 8.—Flow lobe in basin north of King for which profiles were measured to obtain thickness of flow. Sun is to left (enlargement of Apollo 16 panoramic camera frame 5000).

selblad photographs (Pike, 1971a). Such studies continued through Apollo 17 using the newer photographs (Wu and Moore, 1972; Moore and Tyler, 1973; Moore and Wu, 1973). Slope-probability distributions measured with the radar and photogrammetry were compared for the first time after Apollo 17 (Moore and Tyler, 1973). As a result of these studies, certain aspects of the slope-probability distributions were found to be similar and others different (Moore and others, 1980).

BISTATIC-RADAR METHOD

In the Apollo radar experiments, radio signals with wavelengths of 13 cm and 116 cm transmitted by the orbiting spacecraft were reflected from the lunar surface and their echoes received on Earth (Tyler and Howard, 1973). The echoes were broadened in doppler according to the roughness of the reflecting area or subspecular area. The area is assumed to be statistically homogeneous in the analysis because echoes near the center of the area are produced exclusively by surfaces with small tilts and echoes from progressively larger distances are produced by surfaces with progressively larger tilts. Thus large tilts from the center are not detected and small tilts at the periphery are not detected. Very large tilts tend to be mixed with and attributed to noise and are not taken into account. These tilts are about 20° and larger so that omission of them in the analyses is not serious for smooth surfaces, but significant errors may occur in very rough lunar highlands. Roughness, expressed as root-mean-square (rms) slopes,[2] is estimated from echo broadening by

[2]Slope and slope-probability distributions used here are unidirectional or traverse slopes. Thus, they are components of slope measured in a vertical plane and differ from adirectional or landing slopes, which are the maximum component of slope at a given point. Slope angles are measured from the local horizontal to the tilted surface.

hand calculations and machine-calculated algorithms (Tyler and Howard, 1973). These two estimates are not necessarily equal (Moore and others, 1976, p. 46). Slope-probability distributions are determined by analyses of the doppler shift of the echo spectra (Parker and Tyler, 1973) summed over 2° of lunar longitude and limited to slope angles less than 20°. Algebraic standard deviations estimated from the slope-probability distributions are normally larger than hand- and machine-calculated rms slopes (Moore and others, 1976, p. 80, 1980). The scale length sampled by the radar is a function of the wavelength of the transmitted signal and surface roughness characteristics (Tyler, 1976). The mean horizontal distance of the scale length for the radar from empirical determinations is about 100 to 300 radio wavelengths (Tyler and others, 1971; Moore and others, 1975).

PHOTOGRAMMETRIC METHOD

In the stereophotogrammetric method, slope-probability distributions are obtained using stereoscopic pairs of lunar topographic, metric, and panoramic camera positive transparencies in the AP/C plotter. Stereomodels were leveled and scaled from auxiliary data derived from orbital support data (National Space Science Data Center, 1972, 1973, 1974). Three elevation measurements are averaged for each of a number of points separated by a fixed horizontal distance along a linear traverse. The fixed horizontal interval will be referred to as slope length (ΔL) in the following discussion; it is roughly equivalent to the scale length of the radar. Use of a fixed horizontal interval is compatible with previous terrain analysis procedures (Pike, 1971a; Rowan and others, 1971; Pike and Rozema, 1975). Repeated elevation measurements are used to estimate the standard error of measurement (S_E), which can substantially affect results under certain circumstances. More than 400 slopes are determined for each slope-probability distribution. Two statistical descriptors commonly used are mean absolute slope ($\bar{X}$) and algebraic standard deviation (σ). Mean absolute slope is the average of all values of absolute slope angle. Algebraic standard deviations are estimated from the cumulative absolute slope-probability distributions and taken as the slope angle corresponding to a cumulative fraction of 0.32 ($\approx$0.3174) when slope lengths are near 25 m. For large slope lengths, mean absolute slopes and algebraic standard deviations are calculated by the U.S. Geological Survey's terrain analysis computer program.

Radar and photogrammetric roughness estimations differ in several ways: (1) Radio waves penetrate the surface during reflections so that the actual surface is not necessarily measured, whereas stereophotogrammetry is beset with measurement errors related to the instrument, operating personnel, illumination conditions, and photographic quality so that measurement of the surface is approximate, (2) the scale length of sampling by the radar is 100 to 300 wavelengths but varies in relation to location in the sample area and surface roughness, whereas the slope length of sampling by stereophotogrammetry is a fixed horizontal interval, (3) the radar selectively samples surface tilts by magnitude according to location in the sampled area, whereas stereophotogrammetry samples surface tilts as they occur along the traverse, (4) regional tilts of the surface at right angles to the flight path may go unrecognized in radar doppler analyses whereas artificial tilts may be introduced in the photogrammetric method by improper leveling, (5) both methods may encounter sampling problems when the scale of roughness is larger than the size of the samples. Despite these differences and problems, the forms of the slope-probability distributions obtained and variation with horizontal scale are in general agreement.

READING ERROR PROBLEM

As an initial test case, slope-probability distributions for Mare Fecunditatis and the Censorinus Highlands were measured using the stereophotogrammetric method and Apollo 16 mapping camera photographs (Wu and Moore, 1972) at a slope length of 500 m. Estimated algebraic standard deviations from the distributions were compared with rms slopes from the Explorer 35 bistatic-radar experiment (Tyler and Simpson, 1970) for which a scale length between 220 m and 660 m should be expected. The results showed that the roughness determined by the photogrammetric method was higher than the radar method by a significant factor of 1.5 but that both methods found the highland area rougher than the maria by a factor of 2.5 (see table below). This difference prompted an investigation of the effect of reading error on stereophotogrammetrically determined slope-probability distributions (Moore and Wu, 1973).

Location	*Radar slope (degrees)*	*Photogrammetry slope (degrees)*
Censorinus Highlands	6	9.1
Mare Fecunditatis	2.4	3.8

In the photogrammetric method, a fictitious roughness of sizeable magnitude can be introduced (Moore and Wu, 1973). Repeated elevation measurements are normally distributed about the true value under ideal conditions that include a large sample size. These normally distributed elevation errors introduce "noise" in

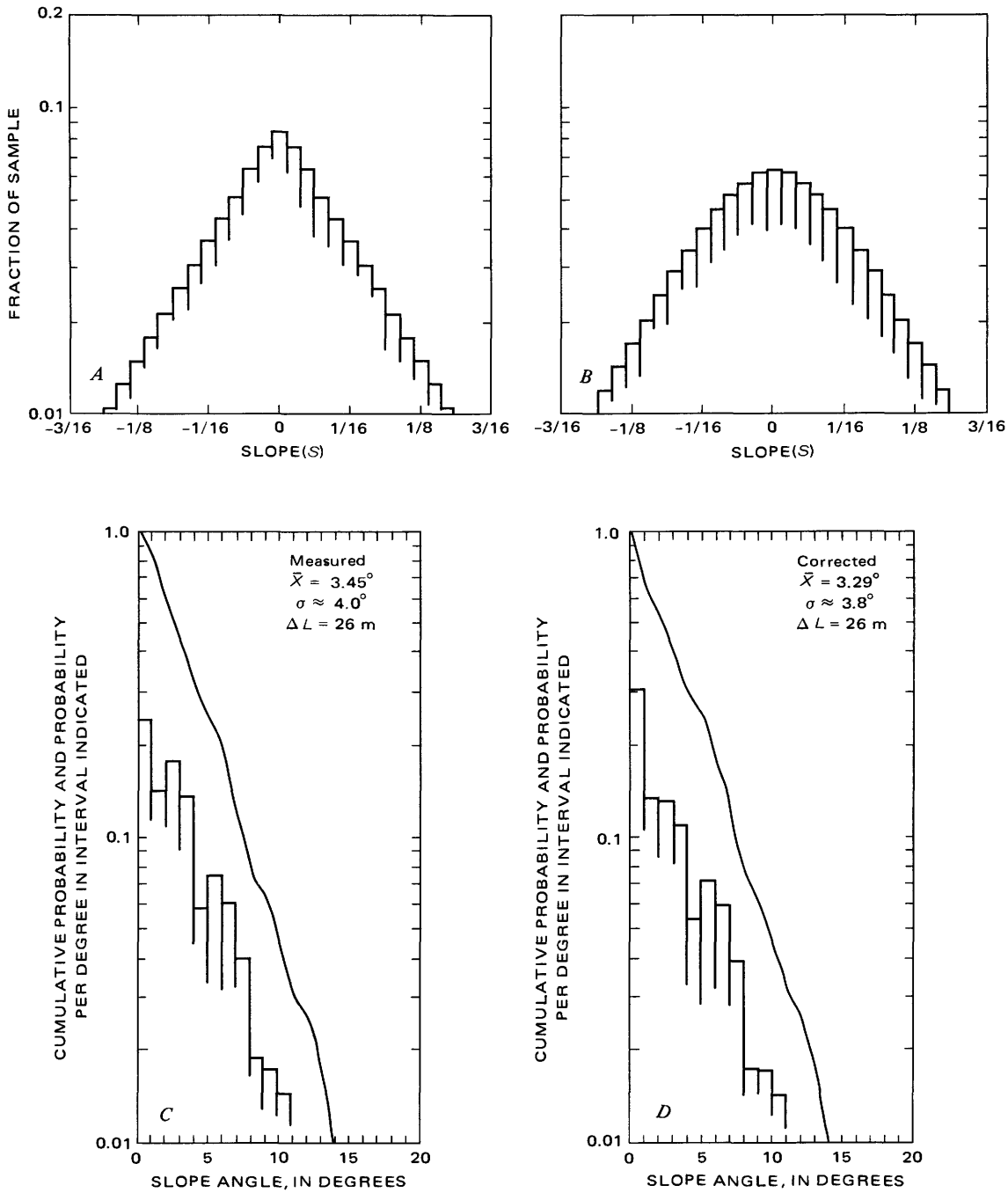

FIGURE 9.—Effect of reading error on semilogarithmic slope-probability distributions. Figure 9*A* shows starting hypothetical distribution. Mean absolute slope is tan 4°. Figure 9*B* shows apparent distribution produced by reading error. Mean absolute slope is tan 4.4°. Notice difference in peakedness of the two distributions. Figure 9*C* shows apparent or measured slope-probability distribution of Cayley plains in lunar highlands. Figure 9*D* shows absolute slope-probability distribution corrected for reading error using practical method of Moore and Wu (1973). Corrected distribution is smoother and more peaked than measured distribution.

the resulting slope probability distribution making the surface appear rougher than it actually is. The general effect is illustrated in figure 9.

Reading errors may produce more pronounced or less pronounced effects on slope-probability distributions depending on the ratio of the slope length and the standard error of elevation difference,[3] ($\Delta L/_{\sigma\overline{\Delta E}}$). For small slope lengths and large standard errors of eleva-

[3]The standard error of the elevation difference ($\sigma_{\overline{\Delta E}}$) is equal to the square root of the sum of the squares of the standard error of the estimate of the mean elevation for each point ($S_{\overline{E}}$), and the standard error of the estimate of the mean elevation is equal to the standard error of measurement (S_E) divided by the square root of the number of measurements in the sample (n).

tion differences, changes are pronounced, whereas for very large lengths and small errors changes are trivial (fig. 10). Application of the general analyses to the Censorinus Highlands and Mare Fecunditatis for reading errors near 10 m and slope-lengths near 500 m places the ratio of $\Delta L/_{\sigma\Delta\bar{E}}$ near 50, and so the differences between the radar and photogrammetry (1.4° and 3°) are too large to be accounted for by reading error.

Most mare surfaces have algebraic standard deviations of 3° to 5° depending on slope length. Thus, slope lengths employed for traverses were guided by reading error. Individual slope-probability distributions at the smallest slope lengths were corrected using the practical method outlined in Moore and Wu (1973). Table 6 summarizes the results of slope probability distributions and their corrections.

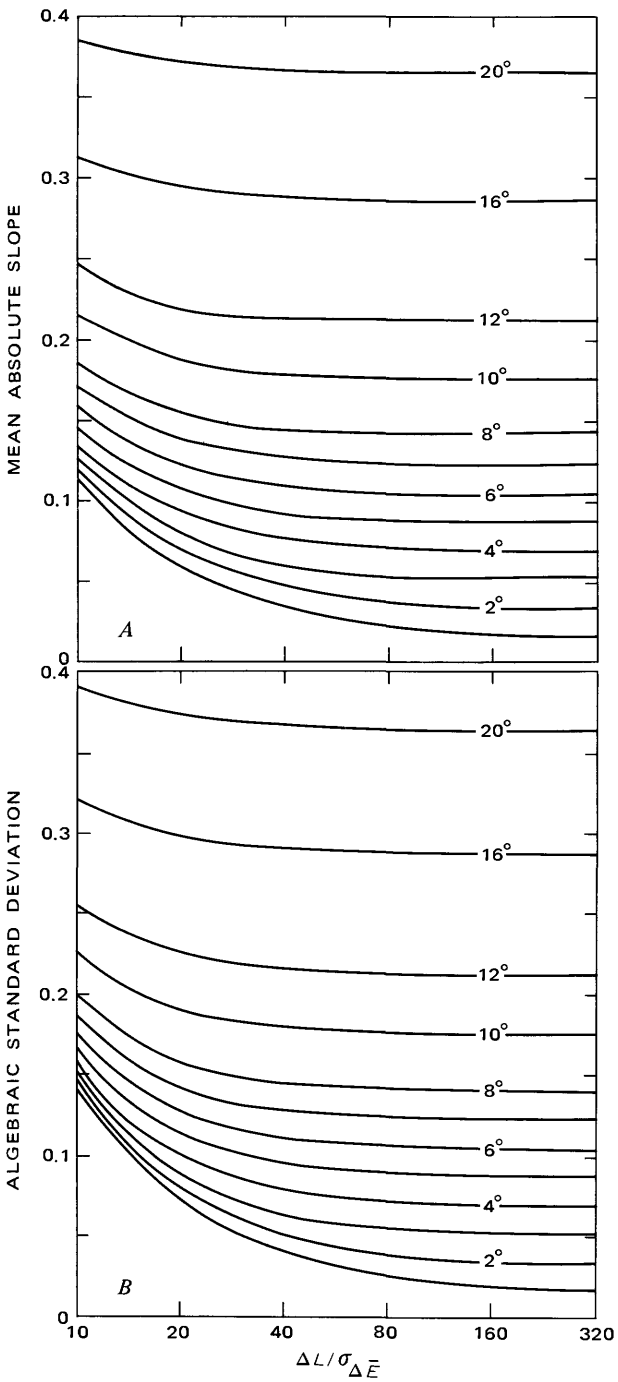

← FIGURE 10.—Effect of photogrammetric reading error on statistical descriptions of slope-probability distribution as a function of slope length (ΔL), standard deviation of elevation difference ($\sigma_{\Delta\bar{E}}$), and surface roughness. *A*, Mean absolute slopes of apparent slope-probability distributions as a function of standard error of slopes resulting from elevation reading errors for semilogarithmic hypothetical slope-probability distributions. Mean absolute slopes for the hypothetical slope-probability distributions are indicated near right ordinate as slope angles. Solid lines indicate apparent mean absolute slopes for various ratios of slope length and standard deviation of elevation differences for adjacent points ($\Delta L\ \sigma_{\Delta\bar{E}}$). *B*, Algebraic standard deviations of apparent slope-probability distributions as a function of standard error of slopes resulting from elevation reading errors for normal or gaussian hypothetical slope-probability distributions. Algebraic standard deviations for the hypothetical slope-probability distributions are indicated near right ordinate as slope angles. Solid lines indicate apparent algebraic standard deviations for various values of the ratio of slope length and standard deviation of elevation differences for adjacent points ($\Delta L/\sigma_{\Delta\bar{E}}$).

RESULTS OF COMPARISON

The radar and photogrammetry methods generally agree on four major points: (1) Maria are smoother than uplands, (2) the magnitude of the algebraic standard deviations derived from the two methods are comparable for the maria, (3) maria appear rougher at small scale lengths than at large scale lengths, and (4) slope-probability distributions are typically semilogarithmic, but they vary and may be gaussian or complex. They disagree on two major points: (1) The roughness of the upland surfaces may appear smaller to the radar at small scale lengths than at large scale lengths, whereas the photogrammetric method shows a larger roughness at a small scale length than at a large scale length, and (2) the magnitude of the radar roughness of the uplands at the small scale length (13-cm wavelength) is low compared to the roughness measured by photogrammetry. Although these results have been discussed previously (Moore and others, 1975, 1976, 1980; Moore and Tyler, 1973), several examples are discussed below.

Comparison of slope-probability distributions of typical maria and the uplands of the Kant Plateau determined by photogrammetry and the radar illustrate the agreement in relative roughness, magnitude of the roughness (algebraic standard deviation), and general agreement in the forms of the distributions (figs. 10, 11, and 12). Perhaps the most important finding by

TABLE 6.—*Statistical parameters of slope-probability distributions using Apollo photographs and stereophotogrammetry*

[σ, algebraic standard deviation; S_E, standard error of measurement; ΔL, slope length]

Location and terrain	Stereophotogrammetric measurements									Photographic measurements					
	Location		Absolute mean, $\bar{X}$ (degree)		ΔL (m)	Estimated σ (degree)	Algebraic mean and type[1]	S_E (m)	Standard error, one slope, S_μ (degree)	Number of slopes	σ (degree)	ΔL (m)	σ (degree)	ΔL (m)	Photograph Nos.
	Long.	Lat.	Corrected	Measured											
Apollo 14 (Lunar Topographic Camera):															
Theophilus, flank near rim	24.9 E	10.7 S	8.75	8.88	25.0	10.8	0.16 G	1.10	1.88	505	5.80	196	3.99	490	80–10501,–10503
Theophilus, flank near rim	24.4 E	10.7 S	6.28	6.45	24.9	7.8	.16 S	.90	2.22	526	4.3	198	2.9	496	80–10504,–10506
Theophilus, ejecta	22.5 E	10.3 S	6.20	6.28	24.5	7.8	.15 G	.54	1.22	517	5.0	196	3.9	490	80–10542,–10544
Theophilus, ejecta	22.4 E	10.3 S	7.30	7.40	23.0	9.0	.22 G	1.00	1.63	510	4.0	184	2.9	460	80–10544,–10546
Rugged upland (Kant Plateau)	20.5 E	9.9 S	8.37	8.46	17.1	10.9	1.9 G	.59	1.36	503	7.6	137	6.1	344	80–10581,–10583
Rugged upland (Kant Plateau)	20.3 E	9.9 S	9.74	9.80	17.6	12.2	1.8 G	.73	1.62	498	9.5	141	8.6	352	80–10588,–10590
Rugged upland (Kant Plateau)	20.1 E	9.9 S	8.06	8.22	16.3	10.3	.15 C	.60	3.07	513	7.5	130	7.2	326	80–10591,–10593
Cratered upland plain	18.4 E	9.5 S	4.71	4.75	24.8	6.3	.03 C	.34	.75	528	3.9	198	3.0	496	80–10622,–10624
Cratered upland plain	18.2 E	9.5 S	5.74	5.82	16.8	6.8	.08 S	.61	1.47	507	2.3	135	1.4	338	80–10624,–10626
Apollo 15 (Panoramic Camera):															
Mare (Serenitatis)	28.1 E	20.0 N	4.70	4.90	25.0	5.9	.51 S	.63	2.02	636	2.3	200	1.4	499	Pan. 9560, 9565
Mare (Serenitatis)	27.5 E	20.2 N	4.78	4.97	24.9	7.0	.42 S	.56	1.79	581	2.5	199	1.3	498	Pan. 9562, 9567
Mare (landing site)	3.7 E	26.1 N	5.64	5.81	25.0	7.0	.04 G	.54	1.73	996	1.5	200	.7	500	Pan. 9809, 9814
Upland (near Proclus)	44.4 E	14.4 N	5.30	5.51	25.1	6.1	1.3 S	.66	2.00	666	4.3	201	3.2	501	Pan. 9508, 9513
Upland (near Vitruvius)	31.3 E	19.2 N	6.17	6.32	25.2	7.6	1.5 C	.95	2.08	622	5.5	202	5.2	504	Pan. 9550, 9555
Rugged upland (Crisium flank)	51.2 E	11.7 N	8.24	8.38	25.2	10.5	2.8 C	1.14	2.00	595	7.8	202	7.3	504	Pan. 9484, 9489
Apollo 16 (Panoramic Camera):															
Mare (Cognitum)	24.4 W	10.3 S	3.12	3.54	25.0	3.9	.14 S	1.10	2.35	654	1.8	200	1.0	500	Pan. 5440, 5445
Cratered plain (in Ptolemaeus)	0.7 W	9.2 S	3.29	3.45	26.0	3.8	.05 S	.86	1.79	631	2.5	208	1.5	520	Pan. 4652, 4657
Uplands (near Capella)	35.4 E	9.0 S	3.81	4.08	25.0	4.7	.39 S	.94	2.08	647	3.6	200	3.2	500	Pan. 4500, 4505
Cratered upland plain (landing site)	15.5 E	8.9 S	5.26	5.53	25.1	6.2	.11 S	.67	2.12	999	4.9	201	3.2	500	Pan. 4558, 4563
Cratered uplands	2.1 E	9.2 S	5.77	5.81	26.1	7.5	1.04 C	.94	1.93	632	6.1	209	5.9	522	Pan. 4644, 4649
Uplands (near Descartes)	16.7 E	9.1 S	6.33	6.71	24.0	8.0	1.31 G	1.07	2.15	656	7.3	192	6.8	480	Pan. 4614, 4619
Uplands (Imbrium sculpture)	6.0 W	9.2 S	7.14	7.39	25.1	8.5	1.46 S	1.12	2.31	609	8.2	201	7.7	504	Pan. 5390, 5395
Apollo 17 (Panoramic Camera):															
Mare (landing site)	30.7 E	20.2 N	3.76	4.05	25.1	4.5	.08 S	.98	2.10	624	2.2	200	1.0	500	Pan. 2750, 2755
Mare (landing site)	30.7 E	20.2 N	3.88	4.19	25.1	4.6	.04 S	1.03	2.18	639	2.7	201	1.2	501	Pan. 2750, 2755
Euler (rim to floor to peak)	29.0 W	23.5 N	14.82	15.38	24.1	18.3	2.49 G			673	15.3	193	14.4	482	Pan. 3105, 3106
Lunar Orbiter:															
Mare (Oceanus Procellarum)	44.1 W	2.6 S	3.45	3.59	17.3	4.1	.69 S	.41	1.29	513	1.3	138	.8	344	LO III H–190,–210
Apollo 16 and 17 (Mapping Cameras):															
Uplands (Censorinus)	31.6 E	4.7 S	7.63	7.73	505	9.0	.02 S	8.39	1.30	1001	----	----	----	----	16M–2167,–2168
Mare (Fecunditatis)	43.5 E	3.2 N	3.10	3.16	500	3.7	.01 S	6.40	1.03	1031	----	----	----	----	16M–2931,–2932
Mixed mare-uplands (Littrow)	30.1 E	20.8 N	5.66	5.86	500	6.4	.13 S	8.51	.92	571	----	----	----	----	17M–0446,–0447
Mixed mare-uplands (Littrow)	30.1 E	20.8 N	5.63	5.70	501	6.3	.01 S	9.23	.98	584	----	----	----	----	17M–1449,–1500
Mixed mare-uplands (Littrow)	30.1 E	20.8 N	4.90	5.06	502	5.5	.03 S	8.87	.95	724	----	----	----	----	17M–2086,–2087

[1]C—complex
G—gaussian distributions
S—semilogarithmic distributions

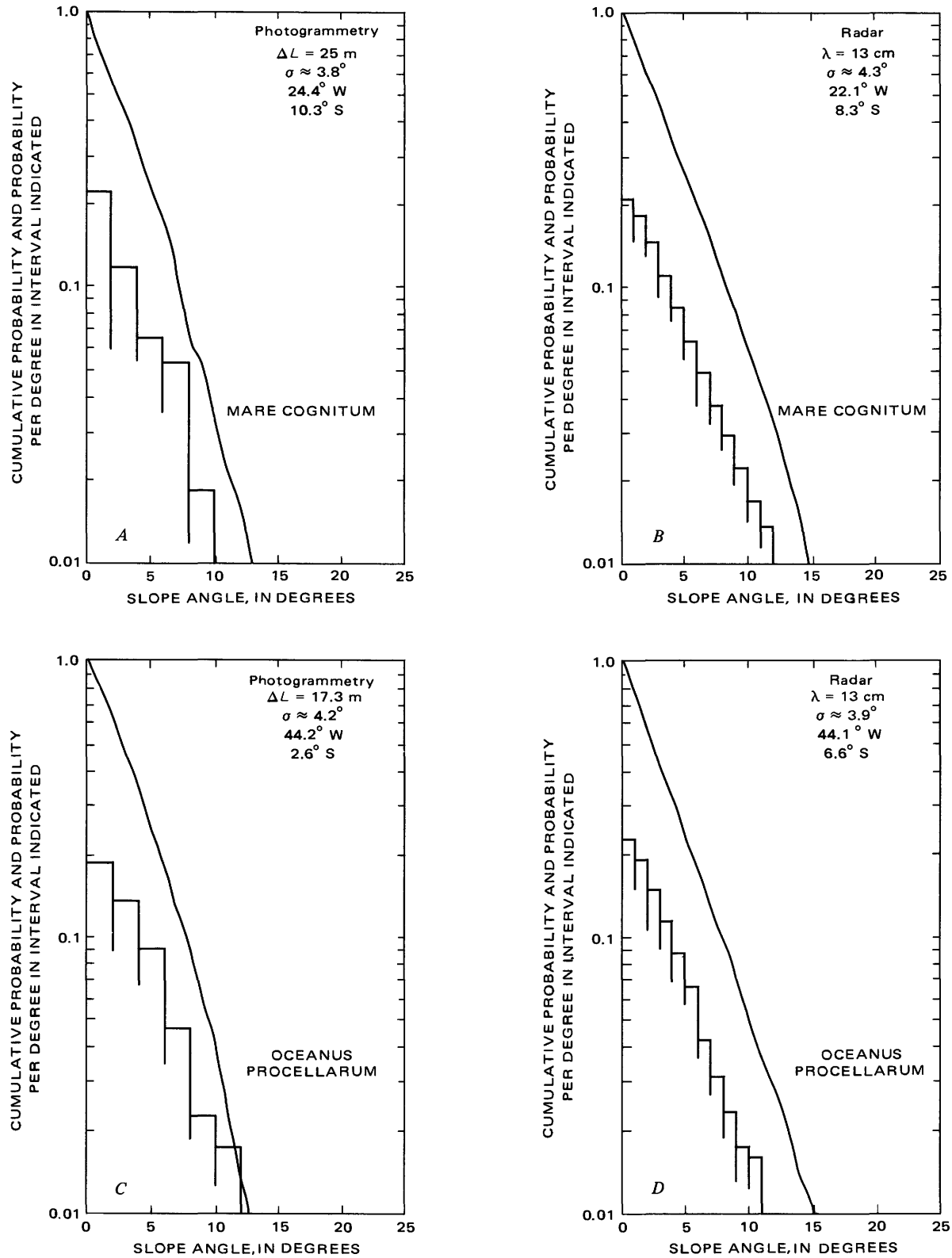

FIGURE 11.—Slope-probability distributions of lunar cratered plains measured by photogrammetry and radar. Distributions found by both methods are very nearly semilogarithmic and estimated algebraic standard deviations are nearly equal. Radar results courtesy of G. L. Tyler, Stanford University.

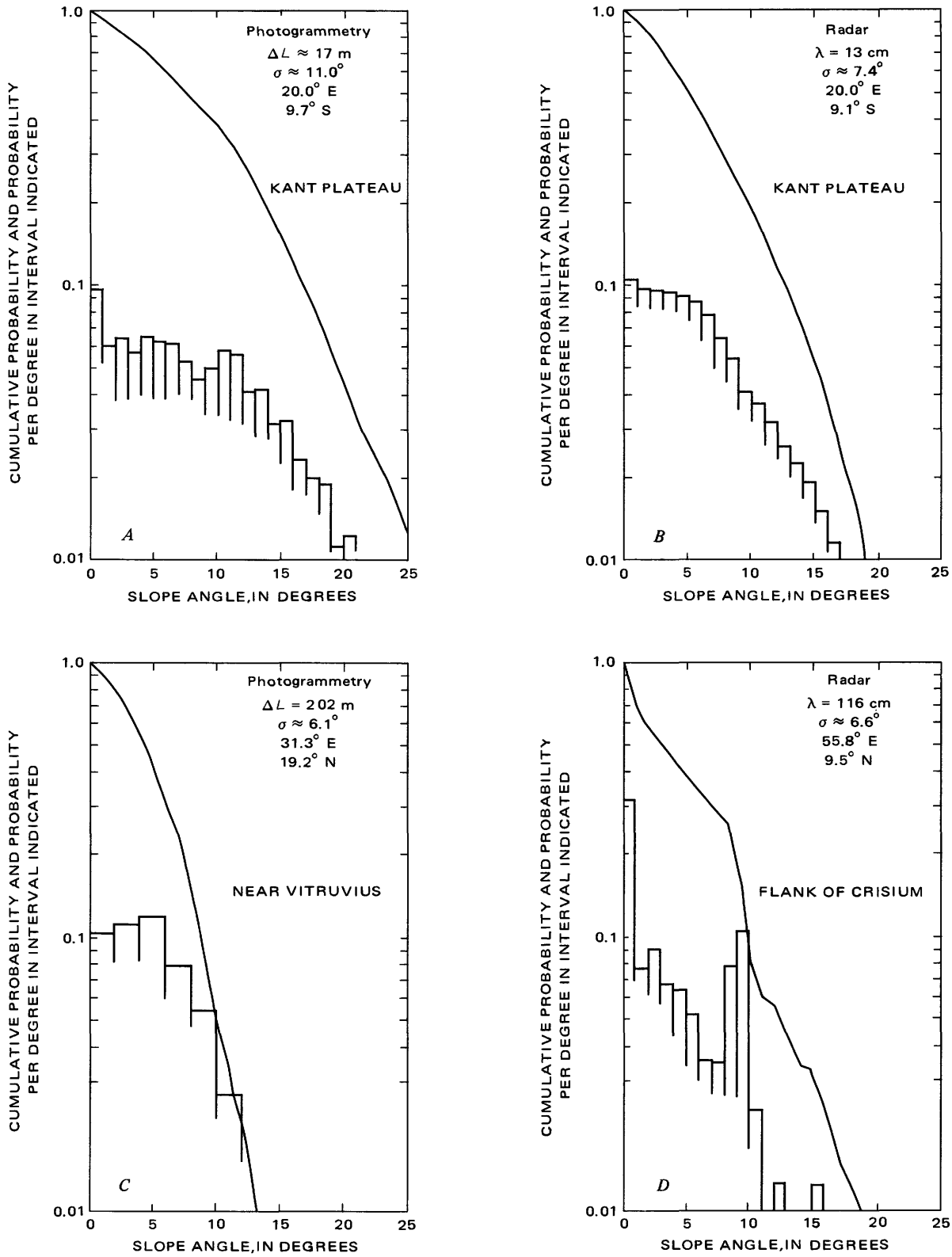

FIGURE 12.—Slope-probability distributions of lunar uplands measured by photogrammetry (*A*, *C*) and radar (*B*, *D*). Kant Plateau distributions (*A*, *B*) approach a gaussian form and those near Vitruvius (*C*) and the flank of Crisium (*D*) are complex. Estimated algebraic standard deviation of Kant Plateau as measured by photogrammetry is larger than that measured by radar. Kant Plateau distribution combines data of three locations in table 6. Radar results courtesy of G. L. Tyler, Stanford University.

both methods is the widespread occurrence of semilogarithmic distributions for cratered mare and upland plains (Moore and others, 1975, 1976, 1980). Such distributions had previously been recognized for cratered lunar plains at smaller scale lengths and found to characterize cratered plains produced by experimental impacts (Moore and others, 1974, and unpublished data). Both methods find distributions different from semilogarithmic in some uplands. These may approach a gaussian distribution or be complex with several modes (fig. 12). Slope-length dependence on roughness as measured by the algebraic standard deviation for single photogrammetric traverses is illustrated in figure 13 (see also table 6), where it may be seen that roughness increases with decreasing slope length (scale length). For the radar, the magnitude of algebraic standard deviation estimated from the distributions may be smaller for the shorter wavelength radar echoes (smaller scale length) than for the large wavelength ones (Moore and others, 1975, p. 83). Root-mean-square slopes of uplands measured by the radar are commonly larger at the large wavelength than at the small wavelength (Moore and others, 1975, 1976). Differences between roughness estimates based on radar and photogrammetry are significant for some uplands such as the Kant Plateau (fig. 12), where photogrammetry estimated the algebraic standard deviation to be 11° and the radar method obtained 7.4° for the smaller scale lengths. In some uplands such as near Vitruvius the two methods agree (Moore and others, 1976, p. 83).

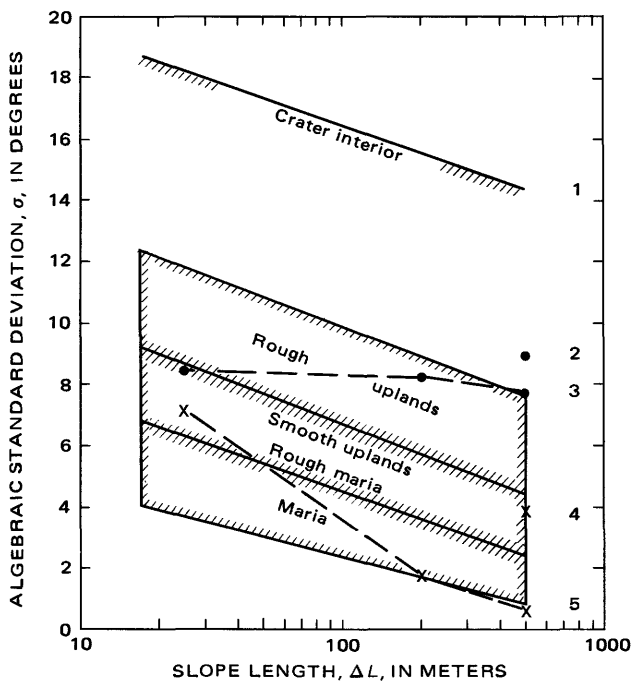

FIGURE 13.—Generalized relations between algebraic standard deviation and slope length as determined using photogrammetric method. Lunar surfaces can be divided into groups: crater interiors, rough uplands, smooth uplands, and maria. Numbers indicate (1) single traverse in interior of Euler from rim to floor to top of central peak (table 6), (2) algebraic standard deviation for Censorinus uplands, from mapping camera photograph (table 6), (3) upland surface (Imbrium sculpture) that deviates from general trend (table 6), (4) algebraic standard deviation for Mare Fecunditatis from mapping camera photographs (table 6), and (5) mare surface that deviates from general trend (Apollo 15 landing site, table 6).

Unresolved problems remain for both methods. In some lunar areas such as the Censorinus Highlands and the south flank of Crisium, the scale length of roughness may exceed the "spot-size" of the radar and the length of the photogrammetric traverses. In these areas as well as the Kant Plateau, many slopes exceed 20° and are not measured by the radar. Although photogrammetry measures slopes greater than 20° along the traverse, very steep slopes are avoided in the selection of a sampling area. These factors may account for the difference in roughness for the Censorinus Highlands measured with the mapping camera and that measured with panoramic camera in the Censorinus Highlands near Capella (table 6). Despite these unresolved problems, current comparisons between the radar and photogrammetry have yielded encouraging results, particularly for the cratered plains, and recognition of the complexity of some upland areas.

CONCLUSION

Apollo orbital photography progressed from unsophisticated systems with valuable but limited measurement capabilities to a sophisticated system with high-quality measurement capabilities. The sophisticated mapping camera system has provided the ingredients for lunar selenodetic control and topographic mapping at scales of 1 : 10,000 to 1 : 250,000. The metric quality of the photographs obtained with the Apollo 14 lunar topographic camera and Apollo 15–17 mapping cameras and panoramic cameras have been profitably used to achieve experimental and scientific objectives. Stereophotogrammetric measurements have been found to be most accurate at sun illumination angles of about 30°. The fine-scale morphology of lunar landforms and structural deformation of the lunar surface can be quantified using topographic maps prepared from the photographs. Equations describing the geometry of lunar craters have been revised because of the topographic maps and profiles prepared from the photographs. Rheological properties of some lunar lava flows have been determined using theory and measurements made from the photographs. Data on lunar surface roughness measured by

stereophotogrammetry form a basis for comparison with results obtained independently by the bistatic-radar experiments.

Full use of the metric quality photographs for some scientific purposes has not been realized. Close coordination between the operator and investigator are required for the purpose. Among the investigations that are incomplete are:

1. A careful study relating stereophotogrammetric measurement with local slopes, the photometric function, and surface albedo.
2. Collection of additional data on crater geometry at the fine scale.
3. Measurements of additional lunar flows.
4. Collection of additional data on lunar surface roughness using a random sampling grid covering a large area comparable to that of the bistatic-radar work.

REFERENCES CITED

Aeronautical Chart and Information Center, 1971, Apollo 14 lunar photography indexes: prepared by Aeronautical Chart and Information center, U.S. Air Force, for Natl. Aeronautics and Space Admin., 3 sheets.

Cannell, W. D., and Ross, C. M., 1976, Development of the Apollo 17 control network: St. Louis, Mo., Defense Mapping Agency, Aerospace Center, Technical Report for NASA contract W–13408, 28 p.

Defense Mapping Agency, Aerospace Center, 1972, Apollo mission 16, lunar photography index maps: prepared and published by Defense Mapping Agency, Aerospace Center, St. Louis, Mo., for the Natl. Aeronautics and Space Admin., 6 sheets.

———1973a, Apollo mission 17 lunar photography index maps: prepared and published by the Defense Mapping Agency, Aerospace Center, St. Louis, Mo., for Natl. Aeronautics and Space Admin., 8 sheets.

———1973b, Lunar topographic orthophotomap, Krieger (1st ed.): LTO 39 A1, scale 1 : 250,000.

———1974a, Lunar topographic orthophotomap, Delisle (1st ed.): LTO 39 B2, scale 1 : 250,000.

———1974b, Lunar topographic orthophotomap, La Hire: LTO 40 A4 (250), scale 1 : 250,000.

———1974c, Lunar topographic orthophotomap, Katchalsky: LTO 65 DZ (250), scale 1 : 250,000.

———1974d, Lunar topophoto map, INA: 41 C3S1 (10), scale 1 : 10,000.

———1974e, Lunar topographic orthophotomap, Nielsen (2nd ed.): LTO 38B2, scale 1 : 250,000.

———1974f, Lunar topographic orthophotomap, Freud (2nd ed.): LTO 38B3, scale 1 : 250,000.

———1975, Lunar topographic orthophotomap, Nielsen (4th ed.): LTO 38B2, scale 1 : 250,000.

Dietrich, J. W., 1971, Photographic summary, *in* Apollo 14 preliminary science report, Part 1: Natl. Aeronautics and Space Admin. Spec. Pub. NASA SP–272, p. 9–31.

Dietrich, J. W., and Clanton, U.S., 1972a, Photographic summary, *in* Apollo 15 preliminary science report, Part 3: Natl. Aeronautics and Space Admin. Spec. Pub. NASA SP–289, p. 3(1) –3(7).

———1972b, Photographic summary, *in* Apollo 16 preliminary science report, Part 4: Natl. Aeronautics and Space Admin. Spec. Pub. NASA SP–315, p. 4(1).

Doyle, F. J., 1963, The absolute accuracy of photogrammetry: Photogrammetric Eng., v. 29, p. 105–108.

Doyle, F. J., Elassal, A. A., and Lucas, J. R., 1976, Selenocentric geodetic reference system: final rept. Natl. Aeronautics and Space Admin. contract T1168B Experiment S–213, Geodetic Research and Development Laboratory, Natl. Oceanic and Atmospheric Admin., and Topographic Division, U.S. Geol. Survey, 53 p.

El-Baz, Farouk, and Head, J. W., III, 1971, Hycon photography of the central highlands, *in* Apollo 14 preliminary science report, Part C: Natl. Aeronautics and Space Admin. Spec. Pub. NASA SP–272, p. 283.

Gardner, I. C., 1932, The optical requirements of the airplane mapping: Bur. Standards Jour. Research, v. 8, p. 445–455.

Howard, H. T., and Tyler, G. L., 1971, Bistatic-radar investigation, *in* Apollo 15 preliminary science report: Natl. Aeronautics and Space Admin. Spec. Pub. NASA SP–289, p. 23(1) –23(10).

Itek Corp., Optical Systems Division, 1967, Optical bar panoramic camera (handbook): Lexington, Mass., Itek pub. 67–3392–2, 33 p.

———1972, Design control specification, mapping camera system: Lexington, Mass., Itek pub. SPG–67–108, 51 p.

Kinsler, D. C., 1975, User guide to 1 : 250,000 scale lunar maps: Houston, Tex., Lunar Science Institute, 24 p.

Kopal, Zdeněk, and Carder, R. W., 1974, Mapping of the Moon—Past and present: Boston, Mass., Reidel Pub. Co., 237 p.

Light, D. A., 1972, Photogeodesy from Apollo: Photogrammetric Eng., v. 38, p. 574–587.

Lucchitta, B. K., 1971, Evaluation of photometric slope deviation, *in* Analysis of Apollo 10 photography and visual observations: Natl. Aeronatics and Space Admin. Spec. Pub. NASA SP–232, p. 31–35.

McEwen, M. C., and Clanton, U.S., 1973, Photographic summary, *in* Apollo 17 preliminary science report, Part 4: Natl. Aeronautics and Space Admin. Spec. Pub. NASA SP–330, p. 4(1)–4(2).

Malhotra, R. C., 1970, Synopsis of camera calibration results for Apollo 14 Hasselblad cameras, *in* Technical report LEC/HASD no. TR–676–20–63: Houston, Texas, Natl. Aeronautics and Space Admin., p. 22.

Moore, H. J., Boyce, J. M., Schaber, G. G., and Scott, D. H., 1980, Lunar remote sensing and measurements: U.S. Geol. Survery Prof. Paper 1046–B, 78 p.

Moore, H. J., Lugn, R. V., and Newman, E. B., 1974, Some morphometric properties of experimentally cratered surfaces: U.S. Geol. Survey Jour. Research, v. 2, p. 279–288.

Moore, H. J., and Schaber, G. G., 1975, An estimate of the yield strength of the Imbrium flows: Proc. Sixth Lunar Science Conf., supp. 6, Geochim. et Cosmochim. Acta, v. 1, p. 101–118.

Moore, H. J., and Tyler, G. L., 1973, Comparison between photogrammetric and bistatic-radar slope-frequency distributions, *in* Apollo 17 preliminary science report, Part C: Natl. Aeronautics and Space Admin. Spec. Pub. NASA SP–330, p. 33(17)–33(26).

Moore, H. J., Tyler, G. L., Boyce, J. M., Shorthill, R. W., Thompson, T. W., Walker, A. S., Wilhelms, D. E., Wu, S. S. C., and Zisk, S. H., 1975, Correlation of photogeology and remote sensing data along the Apollo 14 bistatic-radar ground track, Part I–A working compendium: U.S. Geol. Survey Open-File Rept. 75–284, 88 p.

Moore, H. J., Tyler, G. L., Boyce, J. M., Shorthill, R. W., Thompson, T. W., Wilhelms, D. E., Wu, S. S. C., and Zisk, S. H., 1976, Correlation of photogeology and remote sensing data along the Apollo 14, 15 and 16 bistatic-radar ground tracks, Part II–A working compendium: U.S. Geol. Survey Open-File Rept. 76–298, 101 p.

Moore, H. J., and Wu, S. S. C., 1973, Effect of photogrammetric

reading error on slope-frequency distributions, *in* Apollo 17 preliminary science report, Part 33–C: Natl. Aeronautics and Space Admin. Spec. Pub. NASA SP–330, p. 33(26)–33(34).

National Space Science Data Center, 1969, Lunar Orbiter photographic data: Greenbelt, Md., Natl. Space Sci. Data Center, Data User's Note NSSDC–69–05, 37 p.

———1972, Apollo 15 lunar photography: Greenbelt, Md., Natl. Space Sci. Data Center, Data User's Note, NSSDC 72–07, 58 p.

———1973, Apollo 16 lunar photography: Greenbelt, Md., Natl. Space Sci. Data Center, Data User's Note NSSDC 73–01, 60 p.

———1974, Apollo 17 lunar photography: Greenbelt, Md., Natl. Space Sci. Data Center, Data User's Note, NSSDC 74–08, 68 p.

Norman, P. E., Bender, M. J., and Esten, R. D., 1969, Photogrammetric data reduction, *in* Analysis of Apollo 8 photography and visual observation: Natl. Aeronautics and Space Admin. Spec. Pub. NASA SP–201, p. 64–68.

Ottico Meccanica Italiana S. P. A., 1964, The AS–11A photogrammetric analytical plotter: 81 Via Della Vasca Navale, Rome, Italy, 108 p.

———1966, Analytical plotter-model AP/C, OMI 66-An, 181× 7: 81 Via Della Vasca Navale, Rome, Italy, 77 p.

Parker, M. N., and Tyler, G. L., 1973, Bistatic-radar estimation of surface-slope probability distributions with applications to the Moon: Radio Science, v. 8, p. 177–184.

Pike, R. J., 1971a, Preliminary quantitative terrain-analysis results from three Apollo 10 photographs, *in* Analysis of Apollo 10 photography and visual observations: Natl. Aeronautics and Space Admin. Spec. Pub. NASA SP–232, p. 5–14.

———1971b, Some preliminary interpretations of lunar mass-wasting processes from Apollo 10 photography, *in* Analysis of Apollo 10 photography and visual observations: Natl. Aeronautics and Space Admin. Spec. Pub. NASA SP–232, p. 14–20.

———1972, Crater morphometry, *in* Apollo 16 preliminary science report: Natl. Aeronautics and Space Admin. Spec. Pub. NASA SP–315, part L, p. 29(56)–29(61).

———1973a, Lunar crater morphometry, *in* Apollo 17 preliminary science report: Natl. Aeronautics and Space Admin. Spec. Pub. NASA SP–330, Part A, p. 32(1)–32(7).

———1973b, The lunar crater Linn´e: Sky and Telescope: v. 46, p. 364–366.

———1974, Depth/diameter relations of fresh lunar craters: Geophys. Research Letters, v. 1, p. 291–294.

———1980, Geometric interpretation of lunar craters: U.S. Geol. Survey Prof. Paper 1046–C, 77 p.

Pike, R. J., and Rozema, W. J., 1975, Spectral analysis of land forms: Ann. Assoc. Am. Geographers, v. 65, p. 499–516.

Rowan, L. C., McCauley, J. F., and Holm, E. A., 1971, Lunar terrain mapping and relative-roughness analysis: U.S. Geol. Survey Prof. Paper 599–G, 32 p.

Tyler, G. L., 1976, Wavelength dependence in radio-wave scattering and specular-point theory: Radio Science, v. 11, p. 83–91.

Tyler, G. L., and Howard, H. T., 1973, Dual frequency bistatic-radar investigations of the Moon with Apollos 14 and 15: Jour. Geophys. Research, v. 78, p. 4852–4874.

Tyler, G. L., and Simpson, R. A., 1970, Bistatic radar measurements of topographic variations in lunar surface slopes with Explorer 35: Radio Science, v. 5, p. 263–271.

Tyler, G. L., Simpson, R. A., and Moore, H. J., 1971, Lunar slope distributions; comparison of bistatic-radar and photographic results: Jour. Geophys. Research, v. 76, no. 11, April 10, 1971, p. 2790–2795.

Wildey, R. L., 1972, Physical and geological aspects of heiligenschein measurements, *in* Apollo 16 preliminary science report: Natl. Aeronautics and Space Admin. Spec. Pub. NASA SP–315, Part Y, p. 29–113 to 29–115.

Wilhelms, D. E., 1980, Stratigraphy of part of the lunar nearside: U.S. Geol. Survey Prof. Paper 1046–A (in press).

Wu, S. S. C., 1969, Photogrammetry of Apollo 8 photography, *in* Analysis of Apollo 8 photography and visual observations: Natl. Aeronautics and Space Admin. Spec. Pub. NASA SP–201, p. 68–78.

———1971, Photogrammetry from Apollo 10 photography, *in* Analysis of Apollo 10 photography and visual observations: Natl. Aeronautics and Space Admin. Spec. Pub. NASA SP–232, p. 37–50.

———1976, Illumination and measurement precision for lunar photography: Photogrammetric Eng. and Remote Sensing, v. 42, no. 6, p. 791–801.

Wu, S. S. C., and Moore, H. J., 1972, Frequency distributions of lunar slopes, *in* Apollo 16 preliminary science report, Part 30–C: Natl. Aeronautics and Space Admin. Spec. Pub. NASA SP–315, p. 30(10)–30(15).

Wu, S. S. C., Schafer, F. J., Jordan, Raymond, and Nakata, G. J., 1972, Photogrammetry using Apollo 16 orbital photography, *in* Apollo 16 preliminary science report, Part 30–B: Natl. Aeronautics and Space Admin. Spec. Pub. NASA SP–315, p. 30(5)–30(10).

Wu, S. S. C., Schafer, F. J., Nakata, G. M., and Jordan , Raymond, 1973, Repeatability of elevation measurements Apollo photography, *in* Apollo 17 preliminary science report, Part 33–D: Natl. Aeronautics and Space Admin. Spec. Pub. NASA SP–330, p. 33(35)–33(40).

GPO 689-143